



The Real McCoy: Great Unconformity source-to-sink on the rifted passive margin of Laurentia

Eiel S.C. Anttila^{a,1,*}, Francis A. Macdonald^{a,2}, Joneel Zinto^b, Max D. Britt^c

^a Department of Earth Science, University of California, Santa Barbara, CA 93106, USA

^b Department of Geology, University of Kansas, Lawrence, KS 66045, USA

^c Department of Geosciences, University of Arizona, Tucson, AZ 85721, USA

ABSTRACT

The Great Unconformity separates Archean and Proterozoic basement rocks from overlying Paleozoic sedimentary strata. Hypotheses for the formation of the Great Unconformity make predictions that can be tested within a source-to-sink depositional framework: kilometer-scale exhumation from Neoproterozoic to Cambrian tectonics and dynamic topography predicts protracted delivery of sediments to North American marginal basins, whereas exhumation driven by Cryogenian snowball Earth erosion predicts rapid syn-glacial deposition outboard of snowball Earth ice grounding lines. However, testing these hypotheses in North America is complicated by syn-glacial tectonism. Here, we develop a new depositional model, age model, and tectonic framework for the Trout Creek Sequence and McCoy Creek Group of northeast Nevada and western Utah. We combine geological mapping, stratigraphy, geochemistry, and U-Pb zircon geochronology to demonstrate that these strata represent some of the most distal Neoproterozoic marine deposits preserved on the western margin of Laurentia, and that they were deposited outboard of Cryogenian ice grounding lines. Subsidence modeling supports a ca. 656 Ma Cryogenian rift-drift transition, without requiring an Ediacaran-Cambrian reactivation, which was previously invoked to accommodate the Sauk transgressive sequence on the western Laurentian margin. Nonetheless, sedimentation rates during the Cryogenian snowball Earth glaciations were low, providing a negative test of the sub-glacial erosion hypothesis. Apparent deepening across the glacial intervals, and high sedimentation rates in their aftermath, suggest that Laurentian marginal basins were starved during snowball Earth glaciations. Detrital zircon age spectra through the early Ediacaran McCoy Creek Group display limited up-section variability, consistent with the development and long-term stability of a western Laurentian passive margin and the progressive erosion and redeposition of the Proterozoic sedimentary cover of North America. The dearth of Grenville-age zircon in the uppermost McCoy Creek Group and appearance of jasper clasts derived from Proterozoic units in the Midcontinent, along with detrital mica and carbonate that are the products of first-generation weathering of crystalline basement, are interpreted to be associated with the ca. 570 Ma emergence of the Transcontinental Arch. These data are consistent with thermochronological data documenting diachronous erosion and exhumation across Laurentia over hundreds of millions of years along the Great Unconformity.

1. Introduction

On North America, the Great Unconformity is an unconformable surface separating Archean-Mesoproterozoic basement of the Laurentian craton and overlying Paleozoic sedimentary strata. The Tonian–Middle Cambrian (ca. 1000–510 Ma) lacuna of the Great Unconformity spans the breakup of the supercontinent Rodinia, the assembly of Gondwana, Cryogenian snowball Earth glaciations, the second rise of oxygen, and the origin and diversification of animals. These milestones in Earth history have been variably linked to increased global denudation, weathering, and sedimentation across the Great Unconformity (e.g. Campbell and Squire, 2010; Peters and Gaines, 2012; Husson and Peters, 2017; Keller et al., 2019), yet the timing and mechanisms of the

generation of the Great Unconformity remain unknown. Denudation below the Great Unconformity has been attributed to a variety of driving mechanisms, including exhumation driven by tectonic or geodynamic forcings (Flowers et al., 2020; Sturrock et al., 2021; Macdonald et al., 2023; Peak et al., 2023) and erosion during snowball Earth glaciations (Keller et al., 2019; McDannell et al., 2022; McDannell and Keller, 2022). Previous efforts to constrain the timing and magnitude of exhumation across the Great Unconformity have focused on thermochronology from the craton, but records of denudation and sedimentation are also preserved on continental margins.

In a source-to-sink framework (e.g. Driscoll and Nittrouer, 2000), the amount of rock exhumed and removed from the continents is balanced by deposition in basins. In the case of the Great Unconformity, the

* Corresponding author.

E-mail address: eaanttila@ethz.ch (E.S.C. Anttila).

¹ Now at the Department of Earth Sciences, ETH Zürich, Switzerland, 8092.

² Now at the Department of Earth and Planetary Science, University of California, Berkeley, 94720.

accommodation space for much of the eroded supracontinental material was provided by the rifted passive margins of Laurentia (Macdonald et al., 2023). End-member hypotheses for the timing of exhumation provide predictions for the timing and tempo of sedimentation recorded in the stratigraphic record of continental margins: snowball sub-glacial erosion predicts Cryogenian syn-glacial peaks in sedimentation rate in marginal marine environments, whereas tectonic and geodynamic exhumation predicts protracted sedimentary delivery to Laurentian marginal basins throughout the late Neoproterozoic and early Paleozoic. However, the feasibility of testing these predictions is challenged by the limited preservation of Tonian-Cambrian deep marine or distal marginal strata, the vast majority of which have been destroyed by later tectonism. Furthermore, quantitative tests of these predictions require i) a distal marine Laurentian margin sequence that ii) spans the Cryogenian, at minimum, iii) can produce an age model with sufficient resolution to quantify sedimentation rates on million-year timescales before, during, and after Cryogenian glaciations, and iv), exists within a broadly-constrained tectonic context. This last point is critical for interpreting variability in sedimentation rates, which can change as a function of tectonically- or eustatically-generated accommodation space.

Strata of the Trout Creek Sequence and McCoy Creek Group (Gp) of northeastern Nevada and western Utah formed in an embayment on the western margin of Laurentia and, along with exposures of the Windermere Supergroup in British Columbia and the Selwyn Basin of the Yukon, preserve the most distal Neoproterozoic deposits in North America (Fig. 1a and b; Macdonald et al., 2023). Broadly, this succession records Cryogenian glaciation (Crittenden et al., 1983; Macdonald et al., 2013) and the break-up of the supercontinent Rodinia (Bond et al., 1985; Yonkee et al., 2014; Macdonald et al., 2023, and references therein). However, a basin analysis of these units has been limited by uncertainties in age, depositional setting, and regional correlations.

Here we combine new geological mapping with sedimentological and stratigraphic data to propose a depositional model for the Trout Creek Sequence and McCoy Creek Gp. New U-Pb geochronology and carbonate chemostratigraphy are integrated into an age model, which we use to build a new regional correlation framework and assess the tectonic evolution of a portion of the Tonian-Cambrian western Laurentian margin. With the age, depositional environment, and tectonic context of these strata constrained, we examine the timing, tempo, and provenance of sedimentation in the Trout Creek Sequence and McCoy Creek Gp as a source-to-sink test of hypotheses for the formation of the Great Unconformity.

2. Geological background

Late Neoproterozoic strata are present in the deepest structural levels of the Deep Creek, Snake, Schell Creek, and Egan ranges along the Nevada-Utah border (Fig. 1b). Within these ranges, the Trout Creek Sequence and McCoy Creek Gp are preserved as greenschist facies rocks, but are locally upgraded to amphibolite facies around Mesozoic plutons (Miller and Gans, 1989). In the deepest structural levels, metamorphic fabrics consist of an older, east-dipping cleavage and a younger, more pervasive regional west-dipping cleavage, with the west-dipping cleavage recording subhorizontal, layer-parallel simple shear indicating top-to-the-east transport (Miller and Gans, 1989). Significant tectonic attenuation is limited to the northern Snake Range (Wrobel et al., 2021) and the lower units of the Trout Creek Sequence in the Deep Creek Range (Rodgers, 1984; Monroe, 2023). These units were exhumed during extension in the Eocene-Oligocene and Miocene (Miller et al., 1999). Extension was accommodated by westward tilting and down to the east normal faulting (Miller et al., 1999, and references therein).

The Trout Creek Sequence is a ~3500 m-thick package of meta-sedimentary rocks exposed in the Deep Creek Range (Fig. 1b and c) that were divided into seven map units (Misch and Hazzard, 1962). It is overlain by the ~2800 m-thick McCoy Creek Gp, which was defined at

McCoy Creek on the west flank of the Schell Creek Range, and recognized in the southern Snake Range (Misch and Hazzard, 1962), the Deep Creek Range (Rodgers, 1984), at Heusser Mountain in the central Egan Range (Woodward, 1963), the northern Egan Range (Schneck, 1986), and the Pilot Range (Miller and Lush, 1994) (Fig. 1b). Unit correlations within the McCoy Creek Gp have remained uncertain, in part because of inconsistent nomenclature and subdivision (Fig. SM1). To eliminate potential confusion from inconsistent alphabetical unit schemes, we follow the formation nomenclature of Misch and Hazzard (1962) and Schneck (1986), and define two additional formations (Table SM1a,b).

3. Methods

Detailed descriptions of all methods, including geological mapping, carbonate chemostratigraphy, zircon geochronology, and tectonic subsidence modeling, are summarized in the Supplementary Materials.

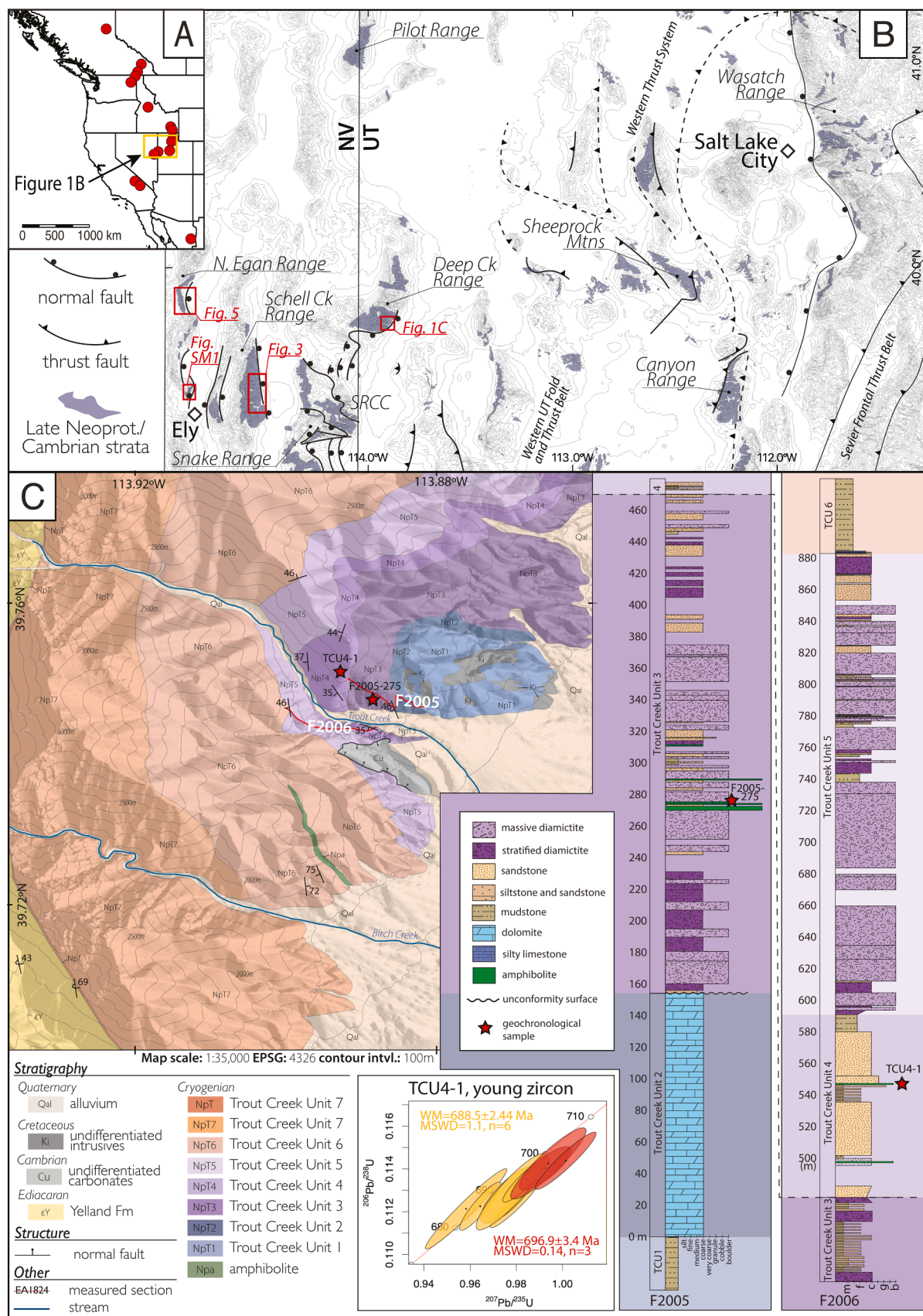
4. Results

4.1. Stratigraphy

4.1.1. Trout Creek Sequence

The Trout Creek Sequence, described by Misch and Hazzard (1962) and Rodgers (1984), is best exposed at the eponymous type locality (Fig. 1c). At Trout Creek, the top of Unit 1 is composed of argillite, and Unit 2 comprises partially calcitized dolomite that is attenuated to ~50 m around a Mesozoic intrusion, but thickens to 147 m on the ridge north of Trout Creek (Fig. 1c). Unit 1 is gradationally separated from Unit 2 by ~2 m of thin-bedded tan-weathering dolostone intercalated with argillite. Carbonate of Unit 2, which locally preserves mm-scale laminated bedding (Fig. 2a), is sharply overlain by Unit 3, which is composed of graded beds of quartzite, stratified diamictite, and minor amphibolite. The matrix-supported diamictite hosts common faceted clasts composed of quartzite, crystalline basement (Fig. 2b), pelite, carbonate, and amphibolite (Fig. 2c). Stretched clasts in Unit 3 diamictites are interpreted to be the result of layer-parallel simple shear (Monroe, 2023, and references therein), resulting in a minimal reduction in apparent thickness. Unit 4 gradationally overlies Unit 3, and comprises graded beds of quartzite-pelite and minor diamictite with bed-penetrating dropstones (Fig. 2d). Unit 5 has a gradational contact with the underlying Unit 4, comprises the same lithologies as Units 3 and 4, but is more dominated by granite- and orthogneiss-clast diamictite. Unit 5 is capped by a laterally continuous ~0.2–1-m-thick limestone bed (Fig. 2e). Together, Units 3–5 are ~760 m thick. Unit 6 comprises ~400 m of grey-to brick-red-weathering pelitic schist, overlain by 800 m of beige-weathering vitreous quartzite with interbedded pelite (Rodgers, 1984). Unit 7 consists of ~1400 m of cliff-forming (Fig. 2f) quartz arenite with tabular cross-beds and minor conglomerate. In the Deep Creek Range, the top of Unit 7 is marked by <10 m of diamictite with an arkosic wacke matrix and pebble- to cobble-sized clasts of quartzite.

In the Schell Creek Range (Fig. 3), strata previously identified as McCoy Creek Gp Unit A are correlative with the upper portion of Unit 7 of the Trout Creek Gp (Misch and Hazzard, 1962; Fig. SM1). There, the lowest exposures of Unit 7 host two ~30 m-thick medium-gray sucrosic marbles separated by ~10 m of quartzite. The marbles are succeeded by ~250 m of massive and tabular cross-stratified quartz arenite beds. This thick quartzite interval is overlain by ~50 m of pelitic schist and quartzite featuring m-scale channelization and minor quartzite pebble- to cobble-clast conglomerate (Fig. 2g), and an additional ~50 m of m-scale beds of massive and tabular cross-stratified quartzite. The top of Trout Creek Unit 7 in the Shell Creek Range comprises a weakly-stratified 5–25 m thick diamictite (Fig. 2h) with quartzite and crystalline (Fig. 2i) basement clasts ranging in size from pebbles to rare boulders.



(caption on next page)

Fig. 1. A) Locations of Neoproterozoic diamictite-bearing successions (red circles) along the western margin of Laurentia, modified from Macdonald et al. (2023). B) Outcrop belt of the Trout Creek Sequence, McCoy Creek Group, and Cambrian Prospect Mountain Quartzite and equivalents depicted in blue. Locations of Trout Creek Sequence and McCoy Creek Group strata discussed in this paper are indicated with red boxes; all labeled ranges are incorporated into the transect depicted in Fig. 7. C) Geological map of the Southern Deep Creek Range, modified from Rodgers (1984) and Monroe (2023). Stratigraphy of Units 1–6 of the Trout Creek Sequence in the Southern Deep Creek Range is shown at right, with the position of measured sections depicted on the map. The stratigraphic height of sample TCU4–1, sampled from the ridge north of Trout Creek, is correlated to an equivalent height within section F2006 on the basis of lithostratigraphic similarities and map relationships. A concordia diagram of the youngest grains from TCU4–1 is shown in the lower center inset. The weighted mean ages of two distinct populations are shown in red and orange text, and are composed of analyses represented by concordia ellipses of the same color.

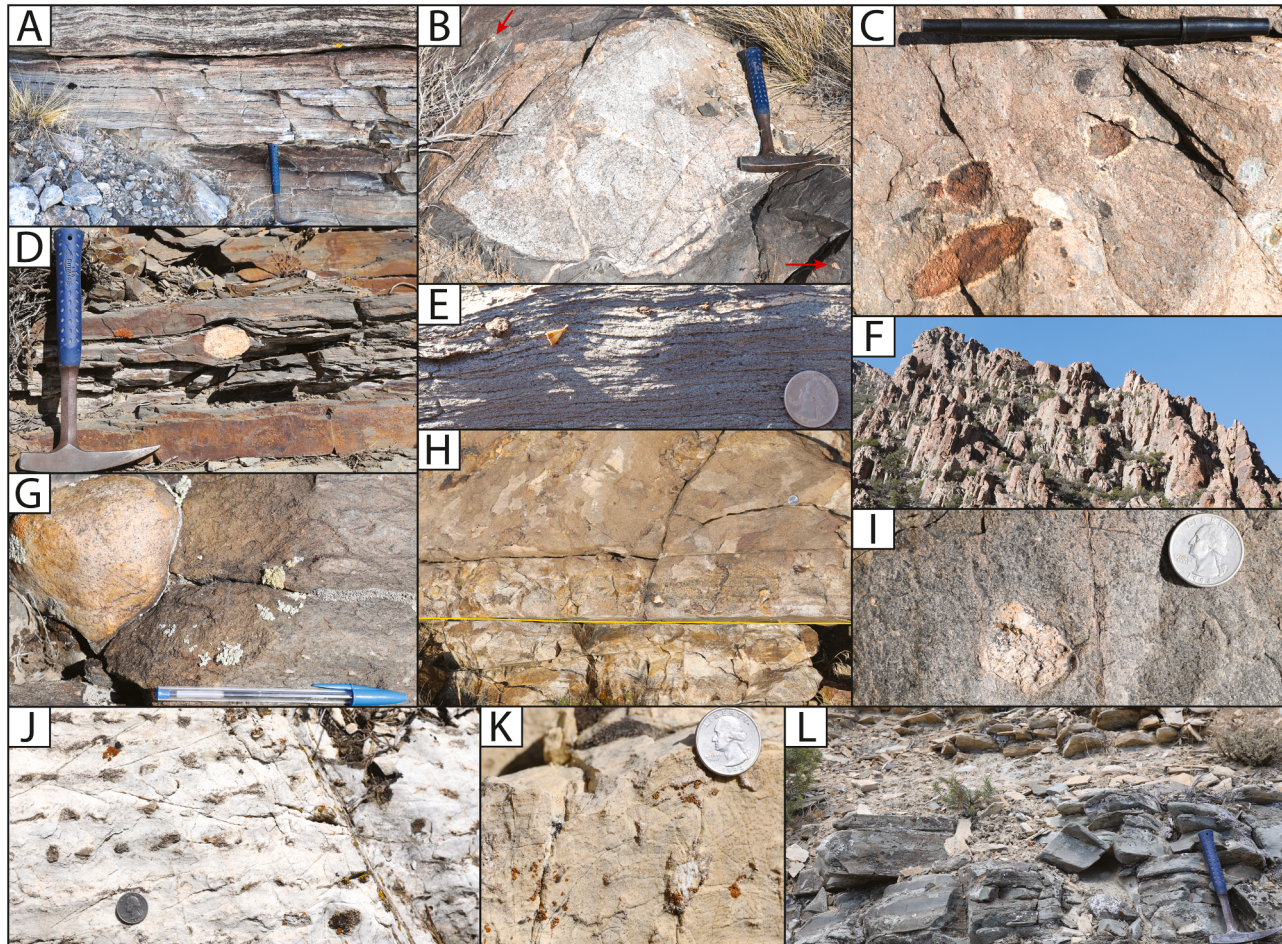


Fig. 2. Field photos of Trout Creek Sequence and basal McCoy Creek Group strata in the southern Deep Creek Range and Schell Creek Range. A) massive weathering, thinly-foliated dolostone of Unit 2 from section F2005; 33cm-long geological hammer for scale. B) Granitic orthogneiss boulder clast in diamictite of Unit 3 from section F2005. Note pebble-to-cobble clasts of quartzites in surrounding outcrop, two of which are indicated with red arrows. 33cm-long geological hammer for scale. C) Amphibolite clasts with reaction rims in Unit 3 diamictite from section F2005. These clasts occur directly above bedding-parallel amphibolite horizons in Unit 3, suggesting that the amphibolites were originally extrusive mafic volcanic material or mafic sedimentary deposits, and not later sills. 15-cm-long pen for scale. D) Gneissic dropstone in laminated fine sandstone horizon within Unit 4; this horizon is ~1 m stratigraphically above the horizon sampled for geochronological sample TCU4–1. 33cm-long geological hammer for scale. E) Basal Unit 6 cap limestone from ridge above section F2005. 2.4-cm-diameter coin for scale. F) Massive ridge forming quartzites of Unit 7, looking from Trout Creek up to northern ridgeline. Vertical relief from photographer's location to the peak at upper left is ~200 m. G) Granite clast in uppermost diamictite of Unit 7 at McCoy Creek, section F2003. 15-cm-long pen for scale. H) Sharp basal contact of uppermost diamictite of Unit 7 overlying clean, bedded quartzites, ridge north of Taft Creek. Contact is indicated with a yellow line; note 2.4-cm-diameter coin in upper right for scale. I) Granite clast in uppermost diamictite of Unit 7 at McCoy Creek, section F2003. 2.4-cm-diameter coin for scale. J) Plan view of tubestone stromatolite in basal cap carbonate of the Yelland Formation at McCoy Creek, section F2003, showing tubes filled with both sparry and micritic cements; 2.4-cm-diameter coin for scale. K) Cross-sectional view of tubestone stromatolite showing faint lamination and funnel-shaped cements, section F2003. 2.4-cm-diameter coin for scale. L) Laminated, sharp-based, graded fine sandstone to mudstone beds and overlying limestones and lutites of Yelland Formation, section F2004. 33cm-long geological hammer for scale.

4.1.2. McCoy Creek Group

The newly-defined Yelland Formation (Fm) (Figs. 1 and 3; Table SM1a) consists of ~200 m of interbedded carbonate and thin graded beds of pelite. A distinctive yellow-white-weathering dolostone of the basal Yelland Fm sharply overlies the uppermost diamictite of Trout Creek Sequence Unit 7 in both the Deep Creek and Schell Creek

Ranges. At McCoy Creek, this interval comprises 11 m of massive and fine-laminated dolostone, with a basal meter-thick horizon of tubestone stromatolites featuring cm-scale sparry to micritic void fill cements that are circular in plan-view (Fig. 2j) and funnel-shaped in cross-section (Fig. 2k). The dolostone interval varies from 0 to 20 m thick along strike, and is overlain by ~20 m of graded fine-grained sandstone, lutite

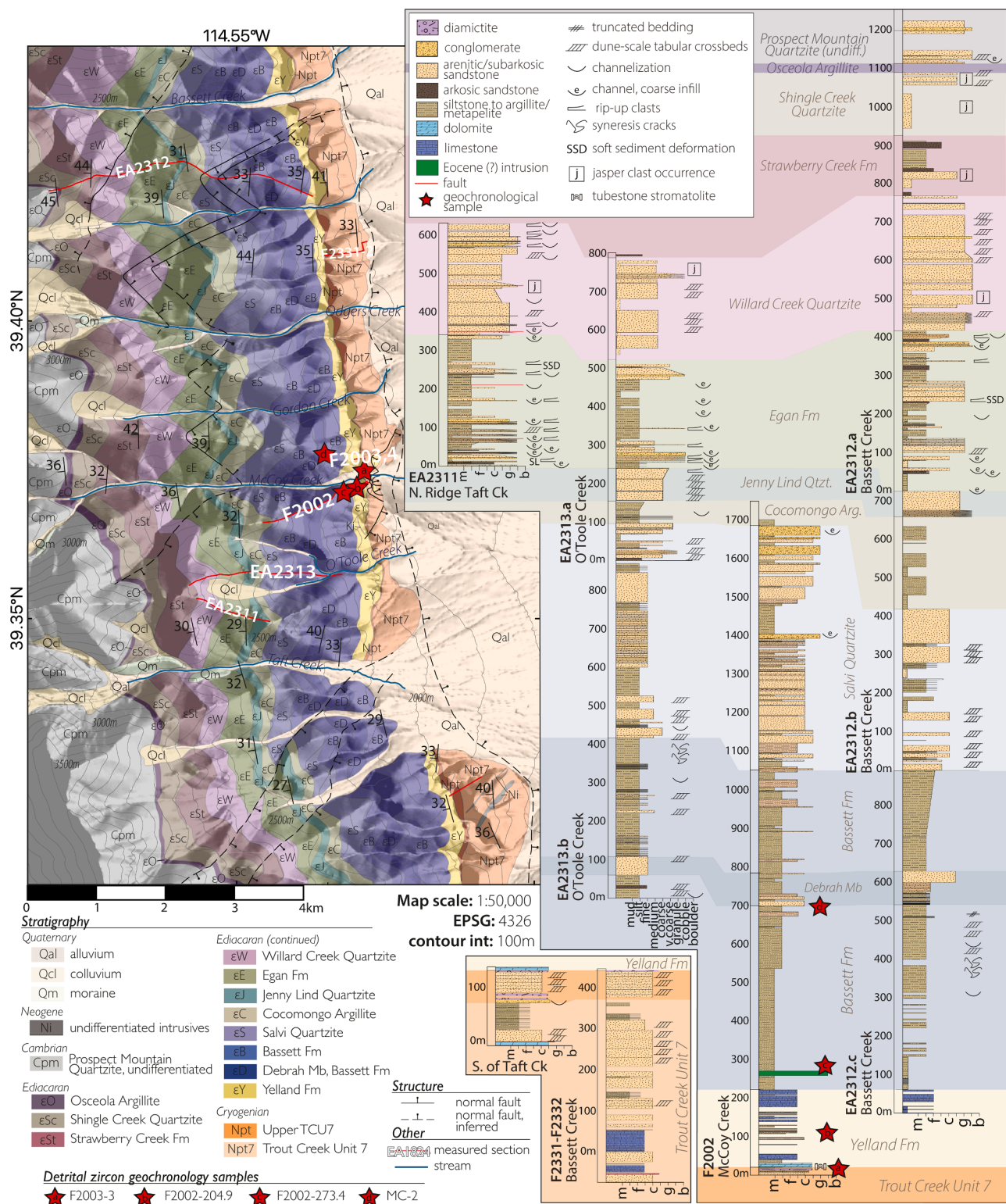


Fig. 3. Geological map of the eastern front of the central Schell Creek Range. Stratigraphy of the McCoy Creek Group is shown at right, with the position of measured sections depicted on the map. Stratigraphy of the upper portions of Unit 7 of the Trout Creek Sequence are shown in the lower central inset panel. Note that stratigraphic repetitions due to map-scale normal faults with well-constrained offsets are not depicted in the plotted stratigraphic sections; faults plotted within the stratigraphic sections are small-offset features observed during section measurement (not visible at map scale). A 1:24,000-scale version of the central Schell Creek Range map is provided in the Supplement.

and limestone (Fig. 2I), and ~100 m of pelitic schist, thin graded beds of sandstone, and allodapic limestone beds.

The newly-defined Bassett Fm (Fig. 3; Table SM1b) comprises ~800 m of fine-grained siliciclastic rocks, with black-weathering phyllite that

becomes increasingly intercalated up-section with cm-thick graded beds of fine- to medium-grained sandstone. The appearance of >1 m thick quartz arenite beds marks the base of the informal Debrah member (Mb; Table SM1b). The Debrah Mb consists of massive, fining-upwards, or

weakly laminated beds of medium-to-coarse grained arenite, laterally discontinuous over 10–100 m distances, that occasionally feature planar dune-scale cross-stratification. The Debrah Mb is overlain by >50 m of pelitic schist featuring abundant syneresis cracks (Fig. 4a) and minor cm-thick graded quartzites.

In the Egan Range, the Salvi Quartzite (Schneck, 1986) comprises ~100 m of resistant medium-grained to granule vitreous gray-weathering quartz arenite with 1–3 m-thick coarse-tail normal

graded beds and tabular cross-beds (Fig. 4b). In the Schell Creek Range, the Salvi Quartzite consists of ~500 m of 1–4 m-thick beds of coarse-grained arenite intercalated with subsidiary fine-grained arenite, phyllite, and slate. Coarse-grained sandstone beds host dune-scale tabular cross stratification and rare intervals of granule-to-pebble quartzite conglomerate featuring erosive bases with up to 50 cm of vertical relief.

The ~50–200 m-thick Cocomongo Argillite (Schneck, 1986)

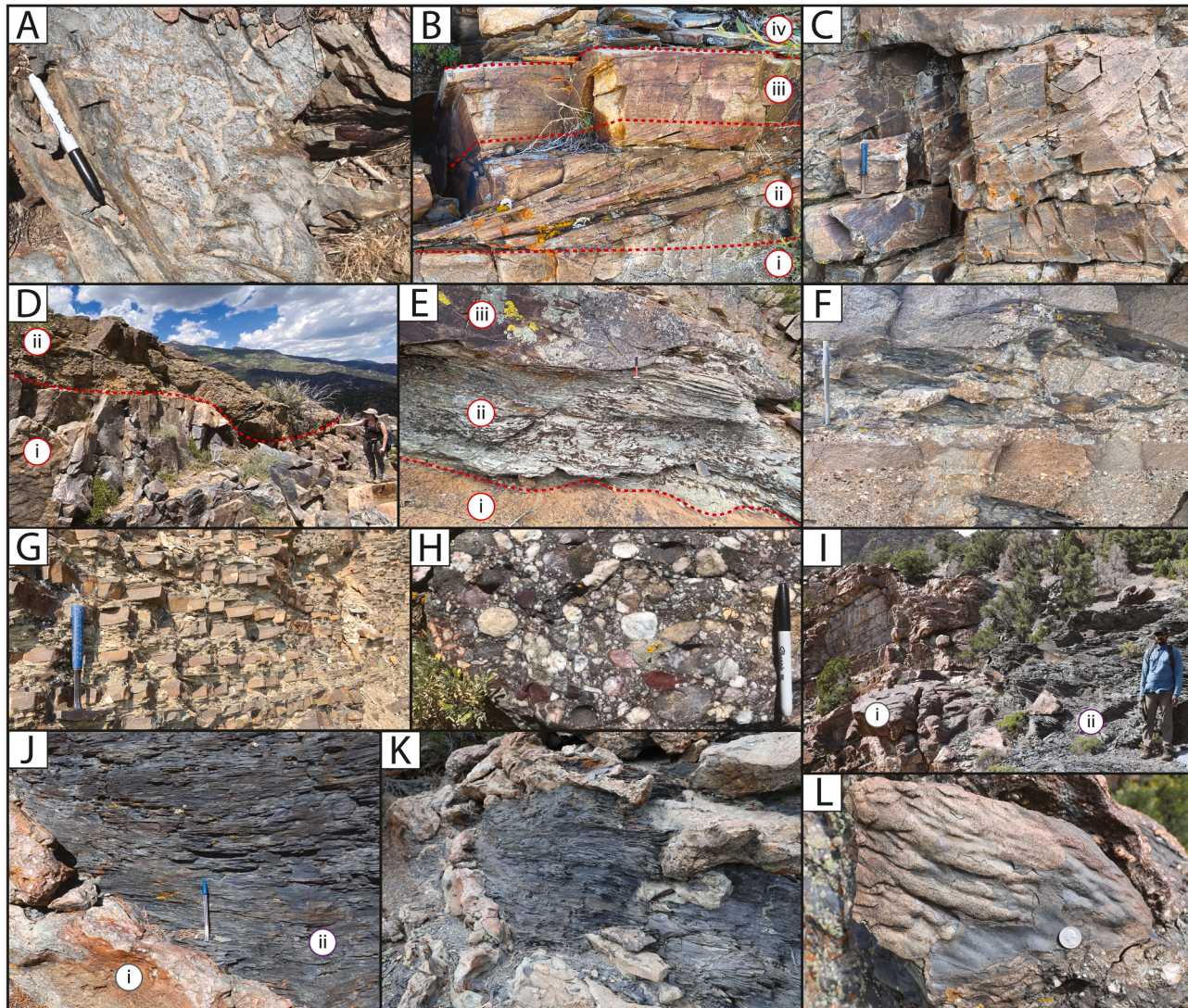


Fig. 4. Field photos of McCoy Creek Group: A) Pervasive syneresis cracks in the Bassett Formation at McCoy Creek, section F2002. 13.7-cm-long pen for scale. B) Fining-upward sandstone package, Salvi Quartzite, McCoy Creek, section F2002. Normal-graded coarse arenite (i) conformably underlies tabular dune-scale crossbeds (ii), laminated fining-upward medium to fine arenite (iii), and laminated fine sand and silt (iv). 2cm-diameter hand lens (just under the boundary of regimes ii and iii, at left) for scale. C) Dune-scale tabular cross-beds in a laterally-discontinuous, m-scale quartz arenite bed, Jenny Lind Quartzite, Taft Creek. 33cm-long geological hammer for scale. D) Channelization at the Jenny Lind-Egan contact, central Schell Creek Range ridge. A ~2 m tall geologist is pointing at an incised channel in the uppermost quartzite of the Jenny Lind Quartzite (i), which is infilled with massive coarse conglomerates of the overlying Egan Formation (ii). E) Basal Egan Formation, northern Taft Creek ridge, section EA2311. An erosional surface above the uppermost Jenny Lind Quartzite (i) is variably overlain by green argillites (ii) and channel- filling quartz conglomerates and coarse quartzites (iii) of the Egan formation. 30cm-long sledge for scale. F) Channel fill, including coarse conglomerates, cobble to boulder rip-up clasts of silt and fine sandstone, and coarse-tail normal graded sandstone (at top). Egan Formation, ridge to north of Bassett Creek. 33cm-long geological hammer for scale. G) Laterally-continuous packages of normal graded 3 cm-thick medium to fine sandstone, overlain by 2–5 cm packages of less-resistant fine sandstone to siltstone of the Strawberry Creek Formation, western ridgecrest of Cocomongo Mountain, northern Egan Range. 33cm-long geological hammer for scale. H) Conglomerate of the Shingle Creek Quartzite, featuring dark jasper clasts, ridge north of McCoy Creek; 13.7-cm-long pen for scale. I) Incised paleotopography cutting into the uppermost Shingle Creek Quartzite (i) in the northern Deep Creek Range. Channel fill deposits of the Osceola Argillite (ii) fill a paleocanyon with ~120 m of relief below a disconformable Shingle-Creek-Osceola contact. 2-m-tall geologist for scale. J) Channels, incised into jasper-bearing conglomerates of the uppermost Shingle Creek Quartzite (i) are infilled by silts and fine sands of the basal Osceola Formation (ii). Northern Deep Creek Range; 15-cm-long pen for scale. K) Osceola channel fill, featuring slump-folded pebble-cobble conglomerate, and coarse sandstone chaotically interfingered with siltstones and shales. From a subsidiary channel within a larger paleocanyon in the northern Deep Creek Range. Note 2.4-cm-diameter coin for scale at photograph center. L) Flute casts, Osceola Argillite, northern Deep Creek Range; 2.4-cm-diameter coin for scale.

coarsens upward from grey argillite to cm-scale graded beds of medium- to fine-grained subarkosic sandstone to siltstone and slate. Rare interstitial intervals of poorly sorted, coarse-grained arenite and granule conglomerate are intercalated within the finer-grained lithologies, and

feature erosive, channelized bases.

The Jenny Lind Quartzite (Schneck, 1986) comprises ~50–115 m of ridge-forming vitreous quartz litharenite featuring 0.5–2 m-thick poorly-sorted sandstone beds with rare tabular dune-scale cross bedding

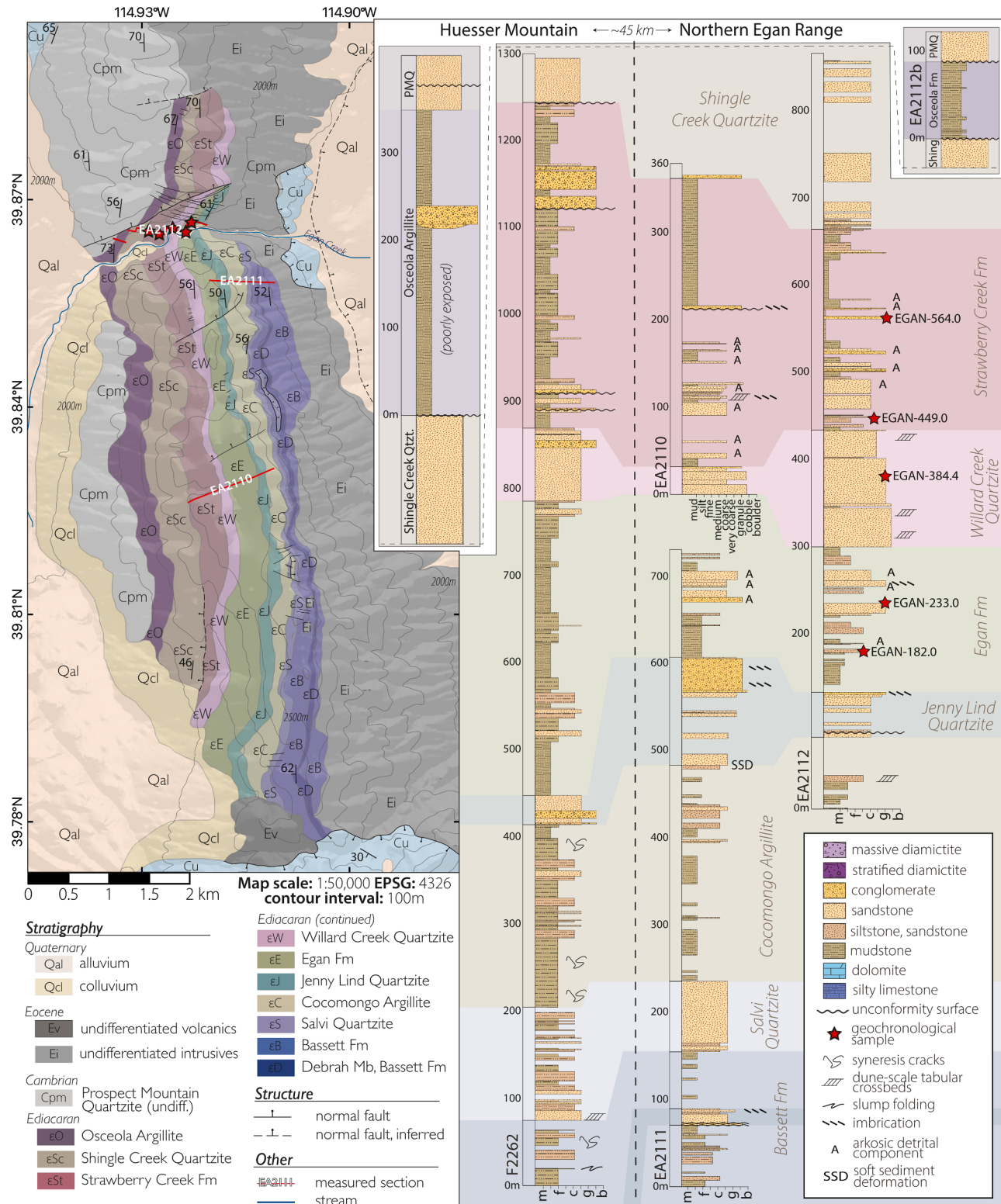


Fig. 5. Geological map of the northernmost Egan Range. Stratigraphy of the McCoy Creek Group is shown at right, with the position of measured sections from the northern Egan Range depicted on the map. Section F2262 and the schematic Osceola Argillite section were measured at Huesser Mountain, ~45 km south of Cocomongo Mountain; a geological map of the Huesser Mountain field area, including the location of Section F2262, can be found in Figure SM2. A 1:24,000-scale version of the northernmost Egan Range map is provided in the Supplement.

(Fig. 4c) and minor partings of sublitharenitic fine-grained sandstone and slate. Incised channels with m-scale vertical relief (Fig. 4d) are common near the top of the unit, which host granule-pebble conglomerate with subangular to rounded clasts of quartzite and slate (Fig. 4e), and abundant slump-folds.

The Egan Fm (Schneek, 1986), comprises a ~165–400 m-thick recessive interval dominated by green slate and argillite, with minor poorly-sorted arkosic to sublitharenitic sandstone in cm- to m-thick graded beds and minor massive granule to pebble conglomerate horizons with channelized bases. The Egan Fm is thickest in the Schell Creek Range, and hosts coarse-grained channel fill deposits with cobble-to-boulder-scale rip-up clasts (Fig. 4f), soft-sedimentary deformation, and slump-folds.

The Willard Creek Quartzite (Misch and Hazzard, 1962; Schneek, 1986) is 30–130 m thick in the Egan Range and 260–340 m thick in the Schell Creek Range. It outcrops as a resistant band of massive, 1–2 m-thick beds of white-weathering vitreous arenitic quartzite with granule-to-pebble quartz conglomerate containing rare dune-scale tabular cross-bedding, pebble stringers, quartz granule to cobble conglomerate, and discontinuous shale partings.

The Strawberry Creek Fm (Misch and Hazzard, 1962) comprises a ~220–350 m, broadly-coarsening-upward sequence of green-blue-gray slate, siltstone, and purple-gray fining-upwards packages of granule conglomerate and arkosic to sublitharenitic sandstone. Channel-filling conglomerates with rip-ups and soft-sedimentary folds are common near the base, while the upper Strawberry Creek Fm contains repeated sharp-based, laterally continuous fining-upwards packages of medium-grained sandstone to siltstone (Fig. 4g).

In the Schell Creek Range, the Shingle Creek Quartzite (Misch and Hazzard, 1962) consists of ~150 m of purple-white-weathering cross-bedded sandstone and quartz and jasper clast pebble conglomerate (Fig. 4h). It varies in thickness from over 540 m at Heusser Mountain (Fig. SM1) to ~100 m in the northern Egan Range (Fig. 5).

The Osceola Argillite (Misch and Hazzard, 1962) is exposed in the northern Deep Creek, southern Snake, Schell Creek (Fig. 3), Egan (Fig. 5), and Pilot Ranges (Fig. 1b). It varies in thickness from ~50–350 m and consists predominantly of micaceous maroon to olive green slate, thin graded beds of sandstone to siltstone, and minor conglomerate and limestone. In the northern Deep Creek Range, purple slate, sandstone, and coarse extra-formational conglomerate fill an incised erosional surface ~120 m deep and 500 m wide (Fig. 4i; Woodward, 1963) at the Osceola-Shingle Creek contact. Conglomerates with quartzite, jasper, and shale rip-up clasts fill subsidiary channels (Fig. 4j and k), while fine-grained sediments host flute casts (Fig. 4l). Above the basal channels, the Osceola Argillite is composed of ~140 m of maroon to olive green slate with thin graded beds of sandstone to siltstone. Stacked channels ~50 m deep and ~100 m wide also occur near the top of the Osceola Argillite, but below the Prospect Mountain Quartzite, and are filled with vitreous quartzite.

In the northern Egan Range, hummocky cross-stratification occurs within slates of the uppermost Osceola Argillite, which are unconformably overlain by conglomerate at the base of the Prospect Mountain Quartzite. In the Pilot Range (Fig. 1b), the upper Osceola Argillite (Miller and Lush, 1994) consists of cm-scale alloclastic limestone beds interbedded with thin white-weathering sandstone and maroon siltstone. Sandstone beds become more common upward, and conformably grade into the white-weathering quartzite of the Stella Lake Quartzite (Misch and Hazzard, 1962), which are integrated (*sensu* Stewart, 1974) within our Undifferentiated Prospect Mountain Quartzite map unit (Figs. 3, 5). The Prospect Mountain Quartzite (Schneek, 1986) variably overlies the Osceola Argillite and Stella Lake Quartzite above an erosional unconformity, and comprises a thick succession of dominantly-arenitic, tan-weathering quartzites that host herringbone cross stratification, lunate ripples exposed on dip-plane surfaces, and flaser bedding within finer-grained intervals.

4.2. Zircon geochronology

Zircon geochronological data are graphically presented in Figs. 1 and 9, and tabulated in Table SM2.

4.3. Carbonate geochemistry

All carbonate geochemical data are graphically presented in Fig. 6, and tabulated in Table SM3.

5. Discussion

5.1. Depositional environments and sequence stratigraphy

5.1.1. Trout Creek Sequence

The bedded diamictite and graded sandstone of Units 3–5 are typical of redeposited glaciomarine subaqueous flow tills that form in front of ice-grounding lines (Domack et al., 1999). Units 3–5 host quartz-rich syn-glacial facies, interpreted as the erosional product of the underlying latest-Tonian Uinta Mountain Gp (Dehler et al., 2010). There is no evidence for local grounded ice, such as ubiquitously massive diamictite or glacio-tectonism, within Units 3–5. Instead, the entire sequence contains graded beds interpreted to represent distal glaciomarine subaqueous deposition below an ice-shelf, offboard an ice-grounding line. However, granite clasts throughout Units 3–5 indicate ice grounding somewhere to the east: predominantly granite clasts in Unit 5 are consistent with subglacial erosion through the Uinta Mountain Gp to basement. Paleocanyons in Big Cottonwood Canyon in the Wasatch Range of Utah are candidate subglacial channels that may have provided basement clasts (Christie-Blick, 1997; Vandyk et al., 2021).

The Unit 5–6 contact records a major sequence boundary interpreted as a post-glacial flooding surface, and marked by a ~20 cm thick cap limestone (Figs. 2e, 6). Unit 6 beds are flat-bedded, graded, and are interpreted to have formed in a depositional environment below storm wave base. A broad coarsening-upward trend continues into Unit 7, where quartzite beds, laterally discontinuous on 10–100 m length scales and bearing dune-scale tabular cross-beds, are intercalated with minor carbonate and channel-fill deposits of quartzite clast conglomerate. However, all unidirectional tabular cross-beds are closely associated with graded beds, and there is no evidence for storm wave base or shoreface deposition in any of these deposits. These facies associations are consistent with deposition within an aggrading shelf margin delta (Porebski and Steel, 2003).

In the Schell Creek Range, the top of Unit 7 reverts to graded beds of pelite with minor diamictite-filled channels, which records glaciation in a pro-grounding line environment. Deglaciation is marked by the return of coarse-grained sedimentation with interspersed diamictite, followed by a glacio-eustatic transgression at the base of the Yelland Fm. The cap dolostone at the base of the Yelland Fm records elevated alkalinity and glacio-eustatic transgression in the aftermath of global glaciation.

5.1.2. McCoy Creek Group

Previous workers have affiliated Neoproterozoic quartzites of western Utah with a fluvial or fluvio-deltaic depositional setting, and posited, without detailed in-situ unit descriptions, that equivalent units in northeastern Nevada were deposited in a similar environment (Christie-Blick 1982; Christie-Blick and Levy, 1989; Levy et al., 1994). Our observations suggest that the majority of the McCoy Creek Group was deposited in a marine shelf margin delta (Porebski and Steel, 2003) below storm wave base. Coarse-grained clastic material was deposited within lobe complexes associated with sediment delivery through submarine canyons and channels amidst a background of fine-grained siliciclastic sedimentation. Quartzite-dominated units of the McCoy Creek Gp vary laterally in thickness from 10 to 100 m across km-scale distances, consistent with lobe complex dimensions in other depositional systems (Porebski and Steel, 2003; Terlaky et al., 2016). Thicker

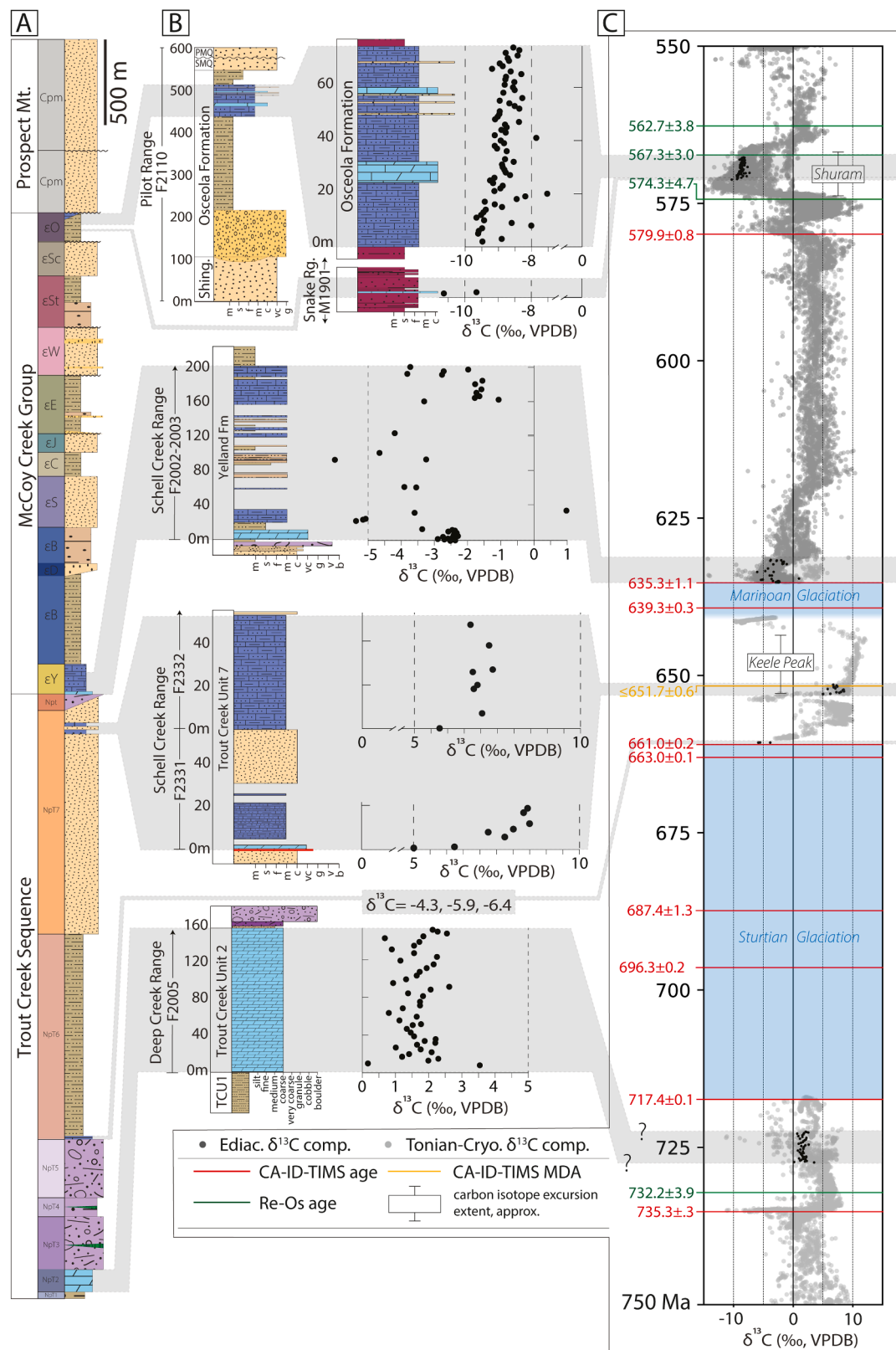


Fig. 6. A) Generalized lithostratigraphy of the Trout Creek Sequence and McCoy Creek Group. A key for lithological symbology can be found in Fig. 3. B) Carbonate $\delta^{13}\text{C}$ chemostratigraphy of the Trout Creek Sequence and McCoy Creek Group, correlated with C) a compiled global Tonian-Ediacaran $\delta^{13}\text{C}$ chemostratigraphy. Radiometric age constraints are depicted as colorful horizontal bars; a version of this figure that includes references for all geochronological constraints and $\delta^{13}\text{C}$ chemostratigraphic compilations is available as Fig. SM3. All chemostratigraphic data from this study, including coordinates of measured sections sampled for chemostratigraphy, are compiled in Table SM3.

quartzite units comprise stacked packages of quartzite beds between 1 and 3 m thick, which feature massive and coarse-tail normal graded beds, beds with dune-scale planar-tabular-crossbedding, and lateral discontinuity across 10–100 m distances. Planar-laminated fine-grained packages are occasionally observed above coarser quartzite packages, (Fig. 4b), corroborating existing models for dune-scale cross-bedding in turbidity currents (e.g. Talling et al., 2012; Terlaky et al., 2016). Similar facies associations of lobe-complex turbidites and subaqueous dunes within Miocene strata of the South China Sea were deposited at depths of

140–200 m (Huang et al., 2021).

In the upper McCoy Creek Gp, quartzite-dominated intervals become thicker, and meter- to decimeter-deep channelization and channel-fill deposits are more frequent, indicating a shift towards up-slope shelf-margin delta facies with increasingly-abundant distributary channels (Porebski and Steel, 2003). This shallowing trend continues through the Osceola Argillite: submarine canyons up to ~100 m deep at the base of the Osceola Argillite host no indication of subaerial exposure below or within the canyon-fill deposits, which include turbidites, debris flows,

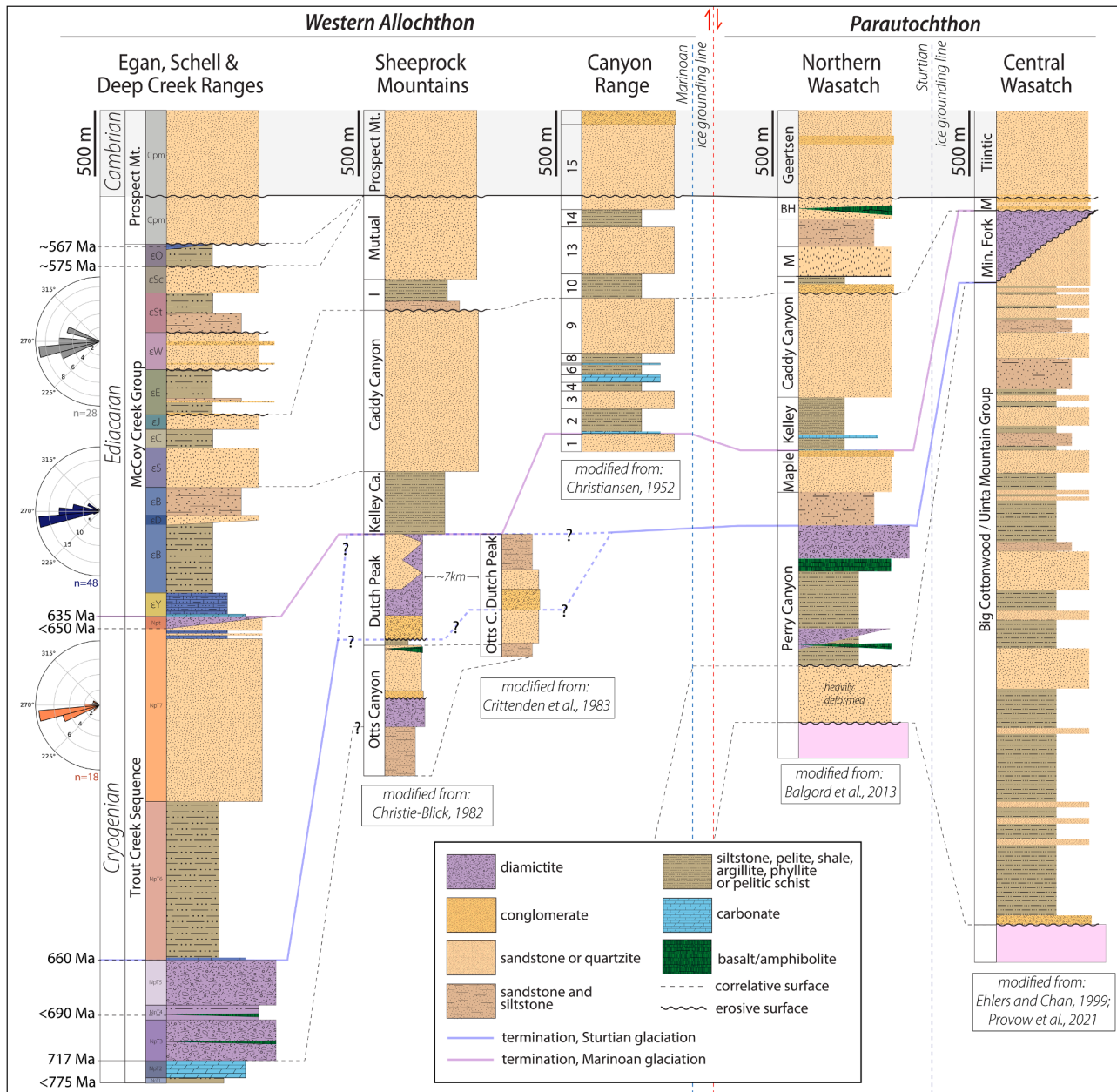


Fig. 7. Regional stratigraphic correlations across an E-W transect from northeastern Nevada to central Utah; allochthonous and parautochthonous localities are separated by the Western Thrust System (e.g. Yonkee et al., 2014), the relative location of which is depicted here with a red vertical dashed line. The locations of each range depicted with a generalized stratigraphic column above are noted in Fig. 1. The inferred relative positions of the Marinoan and Sturtian ice-grounding lines are represented by light- and dark-blue vertical dashed lines, respectively. Note that Marinoan diamictite may be preserved inboard of the Marinoan grounding line in the central Wasatch Range, where the Mineral Fork Fm fills a paleocanyon bounded by an erosive surface that may represent the combined erosive expression of the Sturtian and Marinoan glaciations. Rapid thickness and facies changes (Crittenden et al., 1983) in Cryogenian strata across ~7 km lateral distances in the Sheeprock Mountains complicate correlations with the Trout Creek Sequence; it remains unclear whether the diamictites of the Otts Canyon and Dutch Peak Formations represent two distinct Cryogenian glacial intervals (e.g. Christie-Blick, 1982), or collectively represent the Sturtian glaciation, with thickness variability across the range modulated by Sturtian syn-depositional faulting. Paleocurrent directions from Trout Creek Sequence Unit 7, the lower McCoy Creek Group (Salvi Quartzite and below), and the upper McCoy Creek Group (Jenny Lind Quartzite and above) are depicted with the orange, blue, and gray rose diagrams.

and slump folding (Fig. 4j-l). Imbricate carbonate rip-up clasts and hummocky cross-stratification in the uppermost Osceola Argillite are the only deposits within the McCoy Gp with evidence for deposition above storm wave base. Fluviodeltaic sandstones in the Prospect Mountain Quartzite host flaser bedding, point-bar morphologies, and herringbone cross-stratification, which are absent in the McCoy Creek Gp. The Prospect Mountain Quartzite unconformably overlies either the Stella Lake Quartzite or Osceola Argillite above a low-relief erosional surface, and reflects the culmination of the broad shallowing-upward trend observed throughout the McCoy Creek Gp.

5.2. Age model and regional correlations

The Trout Creek Sequence and McCoy Creek Gp along the Nevada-Utah border are correlative with strata in the Sheeprock Mountains (Christie-Blick, 1982), Canyon Range (Christiansen, 1952), and the northern (Balgord et al., 2013) and central Wasatch Ranges (Ehlers and Chan, 1999; Provow et al., 2021) (Fig. 7). Situated west of the Western thrust system, the Egan, Schell Creek, and Deep Creek ranges, Sheeprock Mountains and Canyon Range are all allochthonous, while parautochthonous sections, separated from the autochthon by the Eastern thrust system, are present in the Wasatch Range (Yonkee et al., 2014).

5.2.1. Tonian

$\delta^{13}\text{C}$ values through Unit 2 of the Trout Creek Gp vary from 0 to +4 ‰ and average +1.8 ‰ (Fig. 6), comparable to values derived from both the Beck Spring Dolomite and the Virgin Spring Limestone in Death Valley, California (Smith et al., 2016). The Beck Spring Dolomite has been correlated via chemostratigraphy and microfossil biostratigraphy to the Callison Lake dolostone in the Yukon, which has been bracketed with Re/Os dates on organic-rich mudstones between 752.7 ± 5.5 and 739.8 ± 6.5 Ma (Rooney et al., 2015). The Virgin Spring Limestone was deposited ca. 732–717 Ma, after the Islay carbon isotope excursion, but prior to the Sturtian glaciation (Smith et al., 2016).

5.2.2. Cryogenian Sturtian glaciation

Units 3–5 of the Trout Creek Sequence were previously interpreted to record two glaciations (Rodgers, 1984). Here, we demonstrate that Unit 4, comprising stratified diamictites, dropstones, and gradational upper and lower contacts, is a quartzite-rich continuation of the glacial facies of Units 3 and 5. Units 3–5 of the Trout Creek Sequence are correlative with ca. 717–662 Ma Sturtian glacial deposits throughout the Cordillera (Figs. 6 and 7), which commonly show evidence for rifting and magmatism (Macdonald et al., 2023; Nelson et al., 2020; Isakson et al., 2022). A volcanoclastic horizon in Unit 4 yielded a young group of 9 zircons, with a population of 3 grains yielding a weighted mean age of 696.9 ± 3.4 Ma, and a population of 6 zircons yielding a weighted mean age of 688.5 ± 2.4 Ma (Fig. 1c). These populations are indistinguishable from CA-ID-TIMS ages on zircon from a tuff below the lower Scout Mountain diamictite of the Pocatello Fm (696.4 ± 0.2 Ma, Isakson et al., 2022) and from the Oxford Mountain locality of the Pocatello Fm (687.4 ± 1.3 Ma; Keeley et al., 2013) respectively, further corroborating the syn-Sturtian affiliation of these strata.

We correlate units 3–5 of the Trout Creek Sequence in the Deep Creek Range with the lower diamictite of the Otts Canyon Fm in the Sheeprock Mountains (Fig. 7). In the northern Wasatch Range, the Sturtian Glaciation is recorded by diamictites of the Perry Canyon Fm (Balgord et al., 2013). In the central Wasatch Range, the Sturtian glaciation is possibly recorded by an erosional unconformity between the uppermost Big Cottonwood Fm and the basal Mineral Fork Diamictite, although the age of the overlying diamictite is unknown. We place the Sturtian ice grounding line outboard of Big Cottonwood Canyon, but east of the allochthonous sections (Fig. 7).

5.2.3. Middle Cryogenian

Unit 6 of the Trout Creek Sequence hosts a basal cap limestone

(Fig. 2e) with $\delta^{13}\text{C}$ values between –4.2 and –6.4 ‰ (Fig. 6), consistent with those derived from ca. 661 Ma Sturtian cap carbonates both regionally and globally (Nelson et al., 2020). Shallowing-upward trends in Unit 6 are paralleled in the northern Wasatch Range, where fine-grained siliciclastic rocks of the uppermost Perry Canyon Fm are found above a carbonate and mudstone sequence that directly overlies the Perry Canyon diamictite (Balgord et al., 2013).

Carbon isotope values from carbonates near the top of Unit 7 of the Trout Creek Sequence that range between +5 and +9 ‰ (Fig. 6) are correlative with the middle Cryogenian Keele Peak carbon isotope excursion, which is also present in the Thorndike submember of the South Park Mb of the Kingston Peak Fm in the Panamint Range of Death Valley (Nelson et al., 2021), stratigraphically below a zircon CA-ID-TIMS maximum depositional age constraint of $\leq 651.7 \pm 0.6$ Ma (Nelson et al., 2020; Fig. 6).

5.2.4. Cryogenian Marinoan glaciation

A Marinoan age for the diamictite at the top of Trout Creek Unit 7 is supported by its position above Sturtian-age deposits and the Keele Peak carbon isotope excursion, its association with the ca. 635 Ma basal Ediacaran cap carbonate (Figs. 2j, k and 6), and its position below a lower Ediacaran transgressive sequence tract (Fig. 7).

In the Sheeprock Mountains, we correlate the Dutch Peak Fm with the Marinoan glaciation (Christie-Blick, 1997), although the basal Ediacaran cap carbonate is absent. In the Canyon Range and northern Wasatch Range in Utah, Marinoan diamictites are not present; the Marinoan horizon is inferred beneath carbonates and fine-grained siliciclastics of Unit 2 of the Canyon Range and the basal Kelly Canyon Fm of the northern Wasatch Range (Balgord et al., 2013). Given the preservation of syn-Marinoan glacial strata without evidence for grounded ice in sections at allochthonous localities, the Marinoan ice-grounding line is inferred to have been located between the restored locations of the Sheeprock Mountains and the Wasatch Range (Fig. 7).

5.2.5. Ediacaran

Unit 7 of the Trout Creek Sequence is capped by dolostone with tubestone stromatolites characteristic of basal Ediacaran cap carbonates (Hoffman, 2011). Furthermore, the carbon isotope profile of the lower Yelland Fm (Fig. 6) is similar to that of the tubestone-stromatolite-bearing Noonday Dolomite of Death Valley (Petterson et al., 2011). The Yelland Fm records a post-Marinoan transgressive sequence that is correlative with slate and carbonate successions of the Kelley Canyon Fm (Fig. 7), which, on Antelope Island in Utah, hosts tubestone stromatolites at its base (Yonkee et al., 2014).

The Salvi, Cocomongo, and Jenny Lind formations, which collectively mark the incipience of abundant coarse-grained clastic sedimentation along the distal margin, are equivalent to coarse-grained siliciclastic rocks of the Caddy Canyon Fm (Christie-Blick, 1982; Provow et al., 2021). Channelization at the Egan-Jenny Lind contact is consistent with regression, which is expressed in more proximal marginal settings as the unconformity above the Caddy Canyon Fm (Levy et al., 1994). Vitreous white quartzites and conglomerates, equivalent to the Willard Creek quartzites, are intercalated with the basal Inkum Fm of the Sheeprock Mountains, and the uppermost channel-fill deposits of the Caddy Canyon described elsewhere in Utah (Levy et al., 1994). Slates of the uppermost Strawberry Creek Fm are correlative with the fine-grained siliciclastic rocks that comprise the majority of the Inkum Fm (Fig. 7). Vitreous quartzite and jasper clast conglomerate of the Shingle Creek Quartzite are the distal equivalent of proximal shelf-shoreface deposits of the jasper-bearing Mutual Fm and equivalents in the Sheeprock Mountains, Wasatch Range, and Canyon Range.

We correlate the erosional incision at the top of the Shingle Creek Quartzite/base of the Osceola Argillite with an unconformity above the Mutual and Browns Hole formations (Fig. 7). In this scenario, the Osceola Argillite has no equivalent in central Utah. The Osceola has been correlated with the Inkum Fm (e.g. Christie-Blick and Levy, 1989),

but this is difficult to reconcile with the strong lithological similarity between the Mutual and Shingle Creek Fms. In either case, canyon cutting events at the base of both the Inkom Fm and the Osceola Argillite cannot have been coeval with paleo-canyon formation at the top of the Johnnie Fm in California (c.f., Giles et al., 2023), as the Osceola Argillite is correlative with the Rainstorm Mb of the Johnnie Fm (e.g. Stewart, 1974). Carbon isotope values in the upper Osceola Argillite (between -11 and $-8\text{\textperthousand}$, Fig. 6) are similar to those of the Rainstorm Mb (Bergmann et al., 2011) and are equivalent to those of the globally-synchronous Shuram negative carbon isotope excursion, which has been constrained by Re-Os geochronology to have occurred between 574.3 ± 4.7 and 567.3 ± 3.0 Ma (Rooney et al., 2020). We suggest that channelization at the top of the Osceola Argillite may be equivalent to canyon incision above the syn-Shuram interval of the Rainstorm Mb.

5.3. Tectonic evolution of the Tonian-Cambrian western Laurentian margin

Previous studies of the McCoy Creek Gp interpreted the stratigraphy as fault repeated (Misch and Hazzard, 1962), resulting in an underestimation of the true stratigraphic thickness. Subsequent studies used these thicknesses and a different age model to infer a failed Cryogenian rift on the western Laurentian margin, followed by a second rift-drift transition in the Ediacaran-Cambrian transition (e.g. Yonkee et al., 2014) to accommodate thick Cambrian successions associated with the Sauk transgressive sequence. Here, we utilize our new age model, new mapping, and measured stratigraphic thicknesses from multiple localities as inputs (Table S4) for a new tectonic subsidence model (Fig. 8a). The resultant tectonic subsidence curve is well-matched (Fig. 8b) by a single idealized thermal subsidence curve (McKenzie, 1978) with a ca. 656 Ma

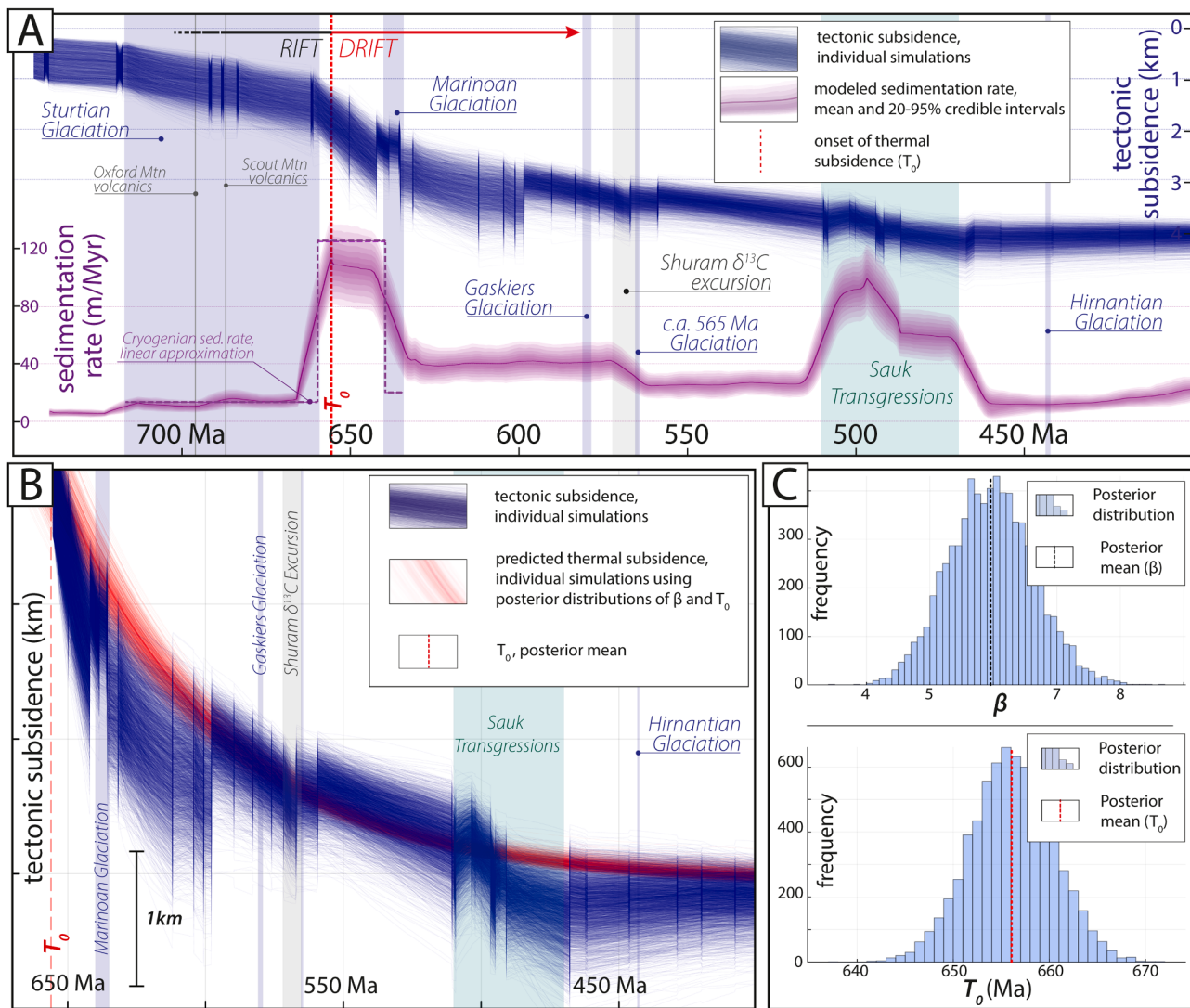


Fig. 8. Model tectonic subsidence and sedimentation rates for the Trout Creek Sequence, McCoy Creek Group, and overlying units. A) A modeled tectonic subsidence curve, comprising 4000 individual Monte Carlo simulations (thin blue lines). Modeled undecompacted sedimentation rates, including the model mean (dark line) and 20 to 95% credible interval envelopes, are depicted in violet. Linear approximations of Cryogenian undecompacted sedimentation rates are depicted with a dashed violet line. The inferred temporal position of the transition from rifting to thermal subsidence along a passive margin (rift-drift transition) is indicated with the vertical red dashed line. B) A late Cryogenian transition from active rifting to thermal subsidence along the margin is corroborated by the exponentially-decreasing rates of tectonic subsidence observed in the Cryogenian-Cambrian modeled tectonic subsidence curve (blue curve), which are coincident with those predicted by idealized thermal subsidence models (sensu McKenzie, 1978), depicted by the red curve, which comprises 1000 individual simulations calculated from distributions of posterior values, output from a Bayesian backstripped tectonic subsidence model, for crustal stretching factor (β) and thermal subsidence initiation (T_0), both of which are shown in panel C). The tectonic subsidence curve can be fit by a thermal subsidence curve with a rift-drift transition c.a. 656 Ma, and a crustal stretching factor of ~ 5.9 . All model parameters and inputs are tabulated in Table SM4. Bayesian age, sedimentation rate, backstripping, and subsidence models utilize the SubsidenceChron.jl (Zhang et al., 2023) framework.

transition from rifting to thermal subsidence, consistent with the presence of ca. 685 Ma volcanism in Idaho (Isakson et al., 2022), and syn-extensional deposition in Cryogenian strata in Death Valley (Macdonald et al., 2013; Nelson et al., 2020). A model β -value of ~ 5.9 is consistent with values expected for attenuated continental-margin-adjacent crust (Roberts et al., 2013). Our findings agree with those of Witkosky and Wernicke (2018), who argued that margin-proximal localities (e.g. Bond et al., 1985; Yonkee et al., 2014) may not fully capture the expression of tectonic subsidence due to the development of unconformities with temporal lacunae of unknown duration, and that more complete, distal Ediacaran successions can account for the apparent misfit between Cryogenian rifting and Cambrian subsidence. Limited Ediacaran-Cambrian volcanism in Utah and Idaho may be far-field expressions of plume activity (Peak et al., 2023, and references therein) or rifting along southern Laurentia (Macdonald et al., 2023). Thus, we infer that the uppermost Trout Creek Sequence, the McCoy Creek Gp, and overlying Cambrian strata were deposited on the thermally-subsiding Nevada-Utah portion of the western Laurentian margin, and that the Sauk sequence was the result of eustasy rather than local tectonic accommodation (e.g. Witkosky and Wernicke, 2018; Tasistro-Hart and Macdonald, 2023).

5.4. Detrital zircon provenance and recycling of Laurentian sedimentary cover

Detrital zircon (DZ) age spectra through much of the upper Trout Creek Sequence and lower McCoy Creek Gp are similar, consistent with deposition along a long-lived Ediacaran passive margin (Fig. 9). Age peaks in the DZ spectra of these rocks (Yonkee et al., 2014), as well as Tonian strata in the Wasatch Range (Dehler et al., 2010; Spencer et al., 2012) have been previously interpreted to indicate the erosion and direct transport of material from basement sources of the same age. However, the presence of an age peak in DZ spectra does not necessitate a single-stage transport pathway between a crystalline basement source and the sedimentary detrital sample, but can instead reflect erosion and redeposition of older strata. Sedimentary sources of the quartzites in the Trout Creek Sequence and McCoy Creek Gp are evidenced by extreme compositional maturity, including through the glacial sequences, and the ubiquity of quartzite clasts. We posit that DZ records of the Trout Creek Sequence and McCoy Creek Gp broadly record the progressive dissection, remobilization, and redeposition of the once-expansive Proterozoic sedimentary cover of Laurentia.

Many of the crystalline basement provinces that make up the core of the Laurentian craton are associated with collisional tectonic events that generated tectonic topography, abundant sediment, and accommodation space, including the ca. 1.6–1.8 Ga Yavapai-Mazatzal Orogeny (Hillenbrand et al., 2023), the ca. 1.3–1.5 Ga Picuris Orogeny (Medaris et al., 2021), and the ca. 0.9–1.3 Ga Grenville Orogeny (Rivers, 2015). These foreland deposits are variably preserved in the stratigraphic record: the superposition of multiple events reworked and redistributed the sedimentary products of earlier collisions. The putative extent of pre- and syn-Grenville sedimentary cover is shown in Fig. 10a.

A prominent Stenian DZ peak is present in most of the Trout Creek Sequence and lower McCoy Creek Gp, suggesting that these strata were derived from the recycling of syn- to post-Grenville sedimentary cover. Cryogenian units of the Trout Creek Sequence may have cannibalized sediments of the Big Cottonwood Canyon Fm and Uinta Mountain Gp (Dehler et al., 2010; Spencer et al., 2012; Yonkee et al., 2014): isolated instances of putatively glacial incision, including a U-shaped canyon with ~ 500 m of vertical relief, cut through the upper portions of these units in the Wasatch Range (Christie-Blick, 1997; Vandyk et al., 2021). Basement-derived clasts within Cryogenian diamictites of the Trout Creek Sequence indicate that syn-glacial erosion encountered crystalline basement along the western Laurentian margin. Canyon incision in the Wasatch Range suggests glacial erosion was focused along ice-streams, analogous to modern Antarctica (Jamieson et al., 2005). Local

basement highs may have also formed due to syn-sedimentary faulting during active rifting.

Following the Cryogenian, DZ spectra throughout the lowermost portions of the McCoy Creek Gp record recycling and redeposition of the Proterozoic sedimentary cover of Laurentia. As Grenvillian-age cover was progressively dissected, underlying sedimentary sources were accessed (Fig. 10b). Rare jasper clasts in quartzites of the Willard Creek Quartzite and Strawberry Creek Fm, and abundant jasper clasts in the Shingle Creek (Fig. 4h) and Osceola formations may provide insight into the increased dominance of pre-Stenian sediment sources: the Sioux Quartzite, found throughout the northern Midwest, is a pre-Grenville red orthoquartzite with abundant jasper clasts (Southwick et al., 1986), and units in Arizona and New Mexico associated with the Mazatzal Orogeny include quartz-jasper conglomerates (Medaris et al., 2021). Within the McCoy Creek Group, as jasper clasts appear and become more common, Stenian detrital zircons disappear.

5.5. Disappearance of Stenian zircons in late Ediacaran and Early Cambrian units

Detrital zircon age spectra from the Osceola Argillite and Prospect Mountain Quartzite conspicuously lack the Stenian peak observed in underlying units of the McCoy Creek Gp (Fig. 9). Similar trends are observed in equivalent units across Utah and southern Idaho (Yonkee et al., 2014). We attribute the dearth of Stenian zircon in these units to the removal of Late Mesoproterozoic and Tonian sedimentary cover, with the exception of outliers preserved in the Midcontinent rift and the ChUMP basins (e.g. Dehler et al., 2010). The emergence of the Transcontinental Arch (TCA, Sloss, 1988; Carlson, 1999) provided a topographic barrier to westerly transport (Brennan et al., 2021) of sediment derived from the midcontinent and Grenville foreland basins. This provenance evolution is consistent with ϵ Nd data from the Trout Creek Sequence and McCoy Creek Group (Farmer and Ball, 1997), which became more negative (evolved) up-section as Stenian cover was removed and Paleoproterozoic basement was progressively exposed. The appearance of mica and carbonate in the Osceola Argillite reflects the regional removal of supracrustal sedimentary cover and the incipience of first-generation chemical weathering and erosion of a basement source. This is further supported by the strong syn-Yavapai basement-age peak observed in the Osceola Argillite DZ spectrum (Fig. 9), as Yavapai basement underlies the western flank of the portion of the TCA that is directly east of the McCoy Creek Gp (Fig. 10a). Thus, the Osceola Argillite records the exhumation of the TCA east of northern Nevada, implying that relative uplift or the generation of topographic relief along this portion of the TCA had occurred by ca. 570 Ma.

The ca. 570 Ma emergence of the TCA recorded in the McCoy Creek Group overlaps with the timing of exhumation of the Canadian Shield inferred from thermochronology (Sturrock et al., 2021; Peak et al., 2023). These studies attributed exhumation to dynamic support associated with plume-related magmatism, including the ca. 610 Ma Central Iapetus magmatic province, the ca. 585 Ma Grenville dikes, the ca. 577 Ma Callander complex, and the ca. 540 Ma Wichita complex (see Peak et al., 2023, and references therein). In this scenario, the progressive Tonian-Ediacaran removal of sedimentary cover west of the TCA axis (Fig. 10b) accelerated ca. 570 Ma in response to dynamic support, creating a continental divide. The TCA axis (Carlson, 1999) broadly traces the known extent of Yavapai basement (Fig. 10a), suggesting that upwelling reactivated preexisting basement structures (Fig. 10b). Variable basement paleotopography, the north-south progression of plume-related magmatism, and the likely-variable thickness of overlying Proterozoic sediments could explain the apparent diachroneity of TCA exhumation, which occurred ca. 525 Ma in Arizona and New Mexico (Holland et al., 2023).

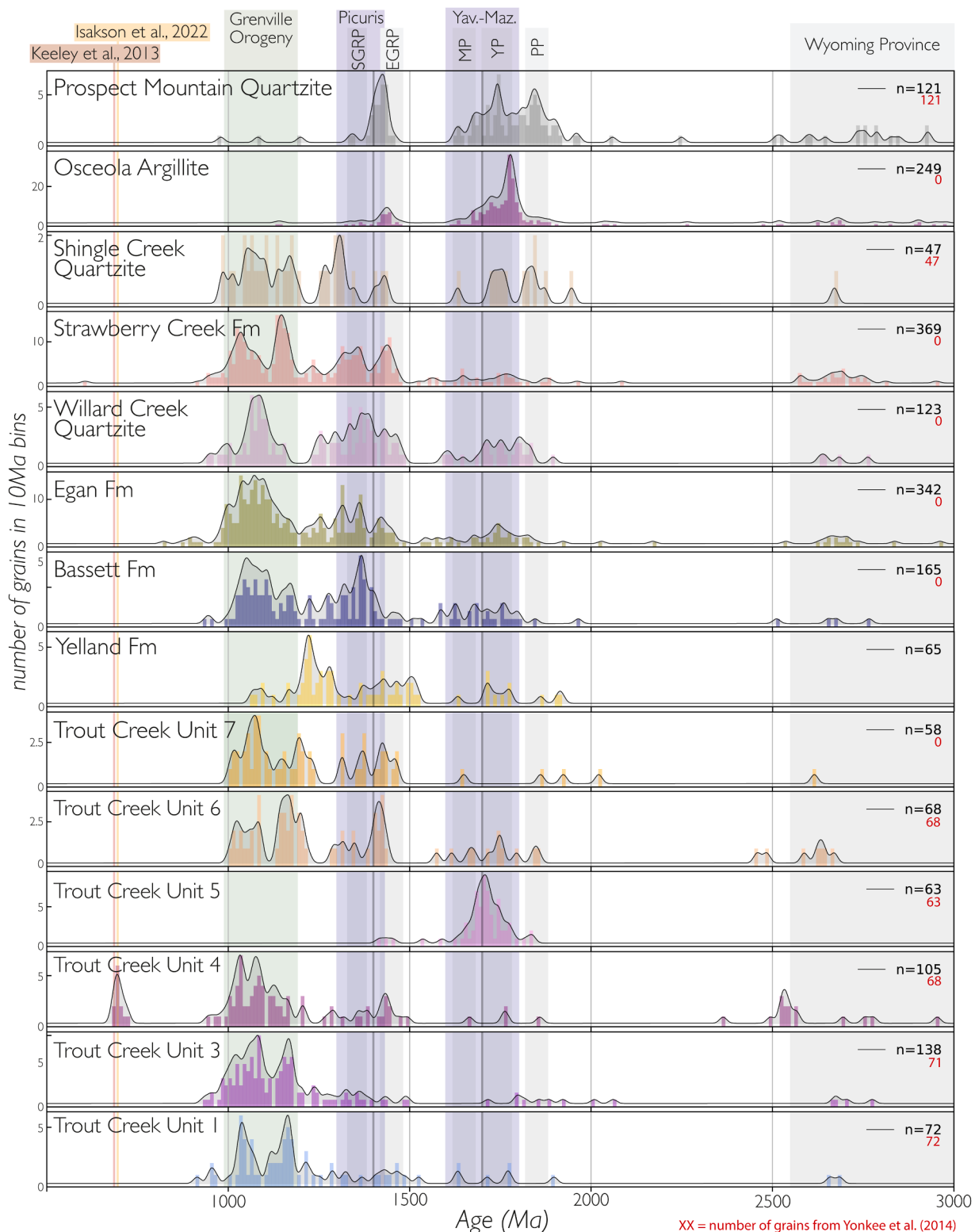


Fig. 9. Normalized age probability density plots depicting the relative abundances of detrital zircon (in 10 Ma age bins) from units within the Trout Creek Sequence, McCoy Creek Group and Prospect Mountain Quartzite. These spectra combine zircon ages developed in this study with extant detrital zircon ages from the Trout Creek Sequence and McCoy Creek Group (Yonkee et al., 2014); red numbers denote the number of grains in the detrital spectrum from the data of Yonkee et al. (2014). All detrital zircon data, including the data of Yonkee et al. (2014) utilized above, are compiled in Table SM2. Note the conspicuous dearth of Stenian, syn-Grenville Orogeny grains in the Osceola Argillite and Prospect Mountain Quartzite. Vertical bars span the putative ages of local volcanic sources (red and yellow bars at left), cratonic basement ages (gray bars at center and right, including the Southern Granite Rhyolite [SGRP], Eastern Granite Rhyolite [EGRP], Mazatzal [MP], Yavapai [YP], Penokean [PP] and Wyoming Provinces) and the durations of putative orogenic events, including the Grenville (green bar), Picuris (left blue bar) and Yavapai-Mazatzal (right blue bar) orogenies. References for basement and orogeny age ranges are tabulated and depicted in Fig. SM4.

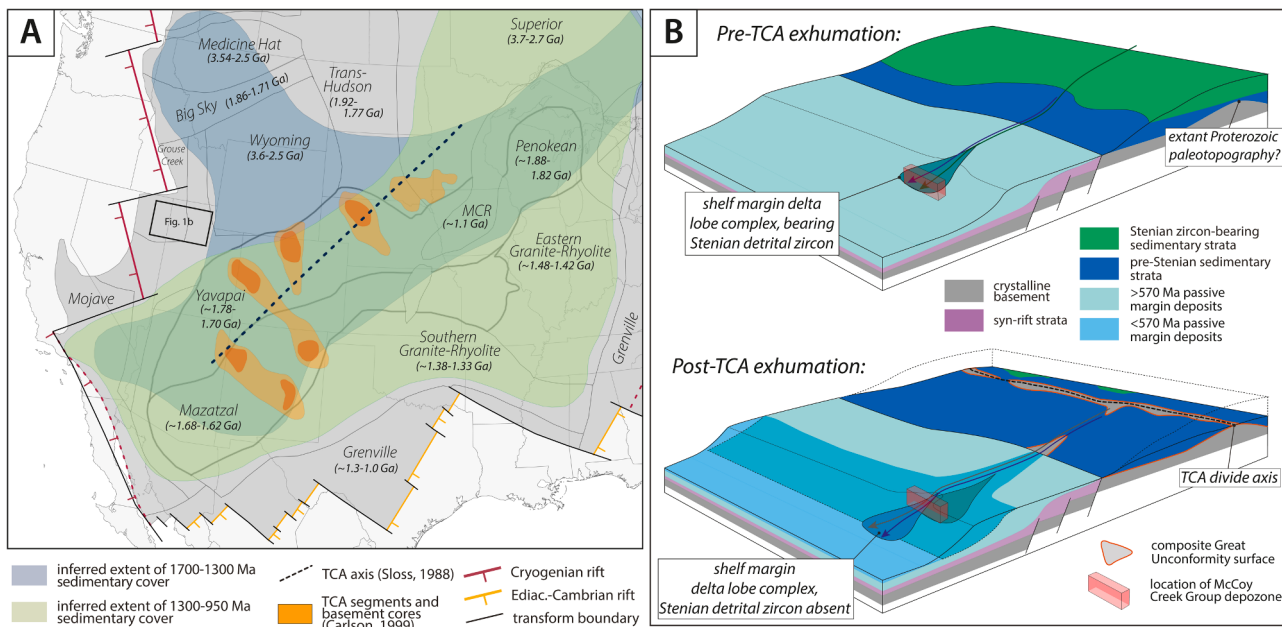


Fig. 10. A) Proterozoic sedimentary cover of Laurentia, depicting the inferred extent of pre-Grenville sedimentary cover (transparent blue polygon) and overlying Grenville foreland deposits and Stenian sedimentary cover (green polygon). A discussion of the approaches used to demarcate these inferred extents, as well as map of the current outcrop extents of Grenvillian and pre-Grenville sedimentary cover, are included in the supplement. Areal extents of basement highs of the Transcontinental Arch (modified from Carlson, 1999) are indicated with orange polygons, with current basement exposures highlighted in darker orange. Note similarities in the trends of the TCA axis (Sloss, 1988) and the approximate axis of the Yavapai and Mazatzal sutures (outlined with bold gray line). A version of this figure, with references used to generate each graphical component, is available in the supplement (Fig. SM4). B) Cartoon depicting the progressive erosion and removal of Grenvillian and pre-Grenville sedimentary cover from the continent, and concomitant deposition of that material along the western Laurentian passive margin. A schematic representation of the depositional environment recorded in our study area is indicated with the red box; note the progressive shallowing of depositional facies due to the gradual progradation of the shelf-margin delta. Erosion of supracrustal sedimentary cover down to preexisting basement structures may have resulted in drainage isolation and the creation of a continental divide (TCA), preventing the westward transport of remnant Grenvillian material from the Mid-continent, and resulting in the dearth of Stenian zircons observed in late Ediacaran-Cambrian strata along portions of the Cordilleran Laurentian margin.

5.6. The distal sedimentary record of great unconformity exhumation

Kilometer-scale Cryogenian sub-glacial erosion (e.g. Keller et al., 2019) predicts the delivery of eroded material to marginal accommodation space. Despite forming along an actively rifting margin, Sturtian glacial strata in the Trout Creek Sequence display meagre undecompressed sedimentation rates of 13.3 m/Myr. Thicknesses of Sturtian glacial deposits from more-proximal localities elsewhere in the Cordillera are highly variable and fault controlled (Macdonald et al., 2023, and references therein), but tend to be <1 km thick, which would result in undecompressed sedimentation rates of <20 m/Myr. Similarly, a conservative linear approximation of syn-Marinoan undecompressed sedimentation rates, utilizing the maximum observed thickness of the Unit 7 diamictite of 100 m and an approximate duration of the Marinoan glaciation of 5 Myr, yields a rate of 20 m/Myr. Marinoan glacial deposits are thin to absent through much of the Canadian Cordillera, but are locally present, with thicknesses also up to 100 m, in the Wildrose diamictite of California (e.g. Nelson et al., 2020), and the upper Scout Mountain member in Idaho (e.g. Isakson et al., 2022). This finding agrees with previous assessments of low sedimentation rates during snowball Earth (Hoffman, 2022; Partin and Sadler, 2016).

The highest sedimentation rates observed in the Trout Creek Sequence and McCoy Creek Gp occur during the middle Cryogenian interval (undecompressed rates of ~125 m/Myr), and can be attributed to the rapid generation of accommodation space due to active rifting and rapid thermal subsidence associated with a ca. 656 Ma rift-drift transition (Fig. 8). Similar thicknesses and a coarsening-upward succession are preserved in the middle Cryogenian of NW Canada in the Twitya and Keele formations (Day et al., 2004). Thick black pelite-dominated successions above the terminations of both Cryogenian glaciations along the Nevada-Utah border are interpreted to reflect basinal starvation,

with sediment supply lagging accommodation space generated by tectonic subsidence and hundreds of meters of relative sea level rise in the wake of the Cryogenian deglaciations. Through both the middle Cryogenian and the Ediacaran succession, facies assemblages record a coarsening up from distal shelf-margin facies to more proximal channelized shelf-margin delta environments, recording the infilling of the starved basins. Accumulation of the thick Ediacaran McCoy Creek Gp along a distal passive margin is the compliment of Ediacaran exhumation and erosion in Laurentia, consistent with the prolonged generation of the Great Unconformity.

6. Conclusions

The Trout Creek Sequence and McCoy Creek Gp of northeastern Nevada and western Utah were deposited on the distal Cordilleran margin of western Laurentia. The Trout Creek Sequence spans the Tonian-Cryogenian periods, whereas the McCoy Creek Gp spans the majority of the Ediacaran. Most of these strata were deposited in a distal shelf-margin environment, with coarse sandstone deposition occurring in lobe-complex deposits. Tectonic subsidence modeling suggests that a single Cryogenian rift, transitioning to a thermally subsiding passive margin ca. 656 Ma, fits the subsidence history of the Nevada-Utah portion of the Cordilleran Laurentian margin, negating the apparent need for reactivation of the western margin to accommodate the Cambrian Sauk sequence.

Low sedimentation rates observed across both Cryogenian snowball Earth glaciations provide a negative test of hypotheses for extensive syn-glacial exhumation and erosion as drivers of the Great Unconformity. Conversely, prolonged delivery of supracrustally-sourced material throughout the Cryogenian and Ediacaran, culminating with source-isolation associated with the ca. 570 Ma exhumation of the

Transcontinental Arch, supports tectonically and geodynamically-forced exhumation and erosion across Laurentia, with the Great Unconformity surface reflecting the amalgamation of erosive events distributed across both space and time.

CRediT authorship contribution statement

Eiel S.C. Anttila: Writing – original draft, Visualization, Validation, Investigation, Funding acquisition, Formal analysis, Data curation, Conceptualization. **Francis A. Macdonald:** Writing – original draft, Supervision, Investigation, Funding acquisition, Conceptualization. **Joneel Zinto:** Writing – review & editing, Investigation, Formal analysis. **Max D. Britt:** Writing – review & editing, Investigation, Formal analysis.

Declaration of competing interest

The authors declare that they have no known competing financial interests or personal relationships that could have appeared to influence the work reported in this paper.

Data availability

All data and code will be made available, upon publication, in a GitHub repository. A link to this repository is supplied in the Supplementary Materials.

Acknowledgments

We thank the University of California Santa Barbara Department of Earth Sciences for support, Ryan Eden, Sam LoBianco and Evan Monroe for their help in the field, John Cottle and Andrew Kylander-Clark for laboratory access and guidance, and Phil Gans for fruitful discussions. We thank Daniel Brennan, Robert Gaines, Brian Wernicke, and an anonymous reviewer for insightful comments that greatly improved the manuscript. ESCA was additionally supported by National Science Foundation (NSF) Graduate Research Fellowship Program (GRFP) 2139319 and NSF Frontier Research in Earth Science (FRES) Grant FRES1925990 to FAM.

Supplementary materials

Supplementary material associated with this article can be found, in the online version, at [doi:10.1016/j.epsl.2024.118852](https://doi.org/10.1016/j.epsl.2024.118852).

References

- Balgord, E.A., Yonkee, W.A., Link, P.K., Fanning, C.M., 2013. Stratigraphic, geochronologic, and geochemical record of the Cryogenian Perry Canyon Formation, northern Utah: implications for Rodinia rifting and snowball Earth glaciation. *Bulletin* 125 (9–10), 1442–1467. <https://doi.org/10.1130/B30860.1>.
- Bergmann, K.D., Zentmyer, R.A., Fischer, W.W., 2011. The stratigraphic expression of a large negative carbon isotope excursion from the Ediacaran Johnnie Formation, Death Valley. *Precambrian. Res.* 188 (1–4), 45–56. <https://doi.org/10.1016/j.precamres.2011.03.014>.
- Bond, G.C., Christie-Blick, N., Kominz, M.A., Devlin, W.J., 1985. An early Cambrian rift to post-rift transition in the Cordillera of western North America. *Nature* 315 (6022), 742–746. <https://doi.org/10.1038/315742a0>.
- Brennan, D.T., Mitchell, R.N., Spencer, C.J., Murphy, J.B., Li, Z.X., 2021. A tectonic model for the Transcontinental Arch: progressive migration of a Laurentian drainage divide during the Neoproterozoic–Cambrian Sauk Transgression. *Terra Nova* 33 (4), 430–440. <https://doi.org/10.1111/ter.12528>.
- Carlson, M.P., 1999. Transcontinental Arch—a pattern formed by rejuvenation of local features across central North America. *Tectonophysics* 305 (1–3), 225–233. [https://doi.org/10.1016/S0040-1991\(99\)00005-0](https://doi.org/10.1016/S0040-1991(99)00005-0).
- Christiansen, F.W., 1952. Structure and stratigraphy of the Canyon Range, central Utah. *Geol. Soc. Am. Bull.* 63 (7), 717–740. [https://doi.org/10.1130/0016-7606\(1952\)63\[717:SASOTC\]2.0.CO;2](https://doi.org/10.1130/0016-7606(1952)63[717:SASOTC]2.0.CO;2).
- Christie-Blick, N., 1982. Upper Proterozoic and Lower Cambrian rocks of the Sheeprock Mountains, Utah: regional correlation and significance. *Geol. Soc. Am. Bull.* 93 (8), 735–750. [https://doi.org/10.1130/0016-7606\(1982\)93.5.735:UPALCR>2.0.CO;2](https://doi.org/10.1130/0016-7606(1982)93.5.735:UPALCR>2.0.CO;2).
- Christie-Blick, N., 1997. Neoproterozoic sedimentation and tectonics in West-Central Utah. *Brigham Young Univ. Geol. Stud.* 42, 1–30.
- Christie-Blick, N., Levy, M., 1989. Concepts of sequence stratigraphy, with examples from strata of late Proterozoic and Cambrian age in the western United States. Late Proterozoic and Cambrian Tectonics, Sedimentation, and Record of Metazoan Radiation in the Western United States: Pocatello, Idaho, to Reno, Nevada 20–29 July 1989. *331, 23–37*.
- Campbell, L.H., Squire, R.J., 2010. The mountains that triggered the Late Neoproterozoic increase in oxygen: the Second Great Oxidation Event. *Geochim. Cosmochim. Acta* 74 (15), 4187–4206. <https://doi.org/10.1016/j.gca.2010.04.064>.
- Crittenden Jr., M.D., Christie-Blick, N., Karl Link, P., 1983. Evidence for two pulses of glaciation during the late Proterozoic in northern Utah and southeastern Idaho. *Geol. Soc. Am. Bull.* 94 (4), 437–450. [https://doi.org/10.1130/0016-7606\(1983\)94<437:EFTPOG>2.0.CO;2](https://doi.org/10.1130/0016-7606(1983)94<437:EFTPOG>2.0.CO;2).
- Day, E.S., James, N.P., Narbonne, G.M., Dalrymple, R.W., 2004. A sedimentary prelude to Marinoan glaciation, Cryogenian (Middle Neoproterozoic) Keele Formation, Mackenzie Mountains, northwestern Canada. *Precambrian. Res.* 133 (3–4), 223–247. <https://doi.org/10.1016/j.precamres.2004.05.004>.
- Dehler, C.M., Fanning, C.M., Link, P.K., Kingsbury, E.M., Rybcyznski, D., 2010. Maximum depositional age and provenance of the Uinta Mountain Group and Big Cottonwood Formation, northern Utah: paleogeography of rifting western Laurentia. *Bulletin* 122 (9–10), 1686–1699. <https://doi.org/10.1130/B30094.1>.
- Domack, E.W., Jacobson, E.A., Shipp, S., Anderson, J.B., 1999. Late Pleistocene–Holocene retreat of the West Antarctic Ice-Sheet system in the Ross Sea: part 2—Sedimentologic and stratigraphic signature. *Geol. Soc. Am. Bull.* 111 (10), 1517–1536. [https://doi.org/10.1130/0016-7606\(1999\)111.5.1517:LPHROT>2.3.CO;2](https://doi.org/10.1130/0016-7606(1999)111.5.1517:LPHROT>2.3.CO;2).
- Driscoll, N., Nittrouer, C., 2000. Source to sink studies. *Margins* 5, 1–3.
- Ehlers, T.A., Chan, M.A., 1999. Tidal sedimentology and estuarine deposition of the Proterozoic Big Cottonwood Formation, Utah. *J. Sedim. Res.* 69 (6), 1169–1180. <https://doi.org/10.2110/jsr.69.1169>.
- Farmer, G.L., Ball, T.T., 1997. Sources of Middle Proterozoic to Early Cambrian siliciclastic sedimentary rocks in the Great Basin: a Nd isotope study. *Geol. Soc. Am. Bull.* 109 (9), 1193–1205. [https://doi.org/10.1130/0016-7606\(1997\)109<1193:SOMPTE>2.3.CO;2](https://doi.org/10.1130/0016-7606(1997)109<1193:SOMPTE>2.3.CO;2).
- Flowers, R.M., Macdonald, F.A., Siddoway, C.S., Havranek, R., 2020. Diachronous development of great unconformities before Neoproterozoic snowball Earth. *Proc. Natl. Acad. Sci.* 117 (19), 10172–10180. <https://doi.org/10.1073/pnas.1913131117>.
- Giles, S.M., Christie-Blick, N., Lankford-Bravo, D.F., 2023. A subaerial origin for the mid-Ediacaran Johnnie valleys, California and Nevada: implications for a diachronous onset of the Shuram excursion. *Precambrian. Res.* 397, 107187. <https://doi.org/10.1016/j.precamres.2023.107187>.
- Hillenbrand, I.W., Karlstrom, K.E., Williams, M.L., Gilmer, A., Premo, W., Davis, P., 2023. Geochemical evidence for evolving Proterozoic crustal thickness and orogenic styles in southwestern Laurentia. *Earth Planet. Sci. Lett.* 622, 118417. <https://doi.org/10.1016/j.epsl.2023.118417>.
- Hoffman, P.F., 2011. Strange bedfellows: glacial diamictite and cap carbonate from the Marinoan (635 Ma) glaciation in Namibia. *Sedimentology* 58 (1), 57–119. <https://doi.org/10.1111/j.1365-3091.2010.01206.x>.
- Hoffman, P.F., 2022. Glacial erosion on a snowball Earth: testing for bias in flux balance, geographic setting, and tectonic regime. *Canadian Journal of Earth Sciences* 60 (7), 765–777. <https://doi.org/10.1139/cjes-2022-0004>.
- Holland, M.E., Mohr, M., Schmitz, M., Madronich, L., Karlstrom, K., 2023. Source-to-sink tandem geochronology reveals tectonic influences on the Cambrian Transcontinental Arch of Laurentia. *Terra Nova*. <https://doi.org/10.1111/ter.12692>.
- Huang, Y., Tan, X., Liu, E., Wang, J., Wang, J., 2021. Sedimentary processes of shallow-marine turbidite fans: an example from the Huangliu Formation in the Yinggehai Basin, South China Sea. *Mar. Pet. Geol.* 132, 105191. <https://doi.org/10.1016/j.marpgeo.2021.105191>.
- Husson, J.M., Peters, S.E., 2017. Atmospheric oxygenation driven by unsteady growth of the continental sedimentary reservoir. *Earth Planet. Sci. Lett.* 460, 68–75. <https://doi.org/10.1016/j.epsl.2016.12.012>.
- Isakson, V.H., Schmitz, M.D., Dehler, C.M., Macdonald, F.A., Adolph Yonkee, W., 2022. A robust age model for the Cryogenian Pocatello Formation of southeastern Idaho (northwestern USA) from tandem in situ and isotope dilution U-Pb dating of volcanic tuffs and epilastic detrital zircons. *Geosphere* 18 (2), 825–849. <https://doi.org/10.1130/GES02437.1>.
- Jamieson, S.S.R., Hulton, N.R.J., Sugden, D.E., Payne, A.J., Taylor, J., 2005. Cenozoic landscape evolution of the Lambert basin, East Antarctica: the relative role of rivers and ice sheets. *Glob. Planet. Change* 45 (1–3), 35–49. <https://doi.org/10.1016/j.gloplacha.2004.09.015>.
- Keller, C.B., Husson, J.M., Mitchell, R.N., Bottke, W.F., Gernon, T.M., Boehnke, P., Peters, S.E., 2019. Neoproterozoic glacial origin of the Great Unconformity. *Proc. Natl. Acad. Sci.* 116 (4), 1136–1145. <https://doi.org/10.1073/pnas.1804350116>.
- Keeley, J.A., Link, P.K., Fanning, C.M., Schmitz, M.D., 2013. Pre-to synglacial rift-related volcanism in the Neoproterozoic (Cryogenian) Pocatello Formation, SE Idaho: new SHRIMP and CA-ID-TIMS constraints. *Lithosphere* 5 (1), 128–150. <https://doi.org/10.1130/L226.1>.
- Levy, M., Christie-Blick, N., & Link, P.K. (1994). Neoproterozoic incised valleys of the eastern Great Basin, Utah and Idaho: fluvial response to changes in depositional base level.

- Macdonald, F.A., Prave, A.R., Petterson, R., Smith, E.F., Pruss, S.B., Oates, K., Fallick, A.E., 2013. The Laurentian record of Neoproterozoic glaciation, tectonism, and eukaryotic evolution in Death Valley, California. *Bulletin* 125 (7–8), 1203–1223. <https://doi.org/10.1130/B30789.1>.
- Macdonald, F.A., Yonkee, W.A., Flowers, R.M., Swanson-Hysell, N.L., 2023. Neoproterozoic of Laurentia. Laurentia: Turning Points in the Evolution of a Continent. *Geological Society of America*. [https://doi.org/10.1130/2022.1220\(19\)](https://doi.org/10.1130/2022.1220(19)).
- McDannell, K.T., Keller, C.B., Guenthner, W.R., Zeitzer, P.K., Shuster, D.L., 2022. Thermochronologic constraints on the origin of the Great Unconformity. *Proc. Natl. Acad. Sci.* 119 (5), e2118682119 <https://doi.org/10.1073/pnas.2118682119>.
- McDannell, K.T., Keller, C.B., 2022. Cryogenian glacial erosion of the central Canadian Shield: the “late” Great Unconformity on thin ice. *Geology*. 50 (12), 1336–1340. <https://doi.org/10.1130/G50315.1>.
- McKenzie, D., 1978. Some remarks on the development of sedimentary basins. *Earth Planet. Sci. Lett.* 40 (1), 25–32. [https://doi.org/10.1016/0012-821X\(78\)90071-7](https://doi.org/10.1016/0012-821X(78)90071-7).
- Medaris Jr., L.G., Singer, B.S., Jicha, B.R., Malone, D.H., Schwartz, J.J., Stewart, E.K., Reiners, P.W., 2021. Early Mesoproterozoic evolution of midcontinental Laurentia: defining the geon 14 Baraboo orogeny. *Geosci. Front.* 12 (5), 101174 <https://doi.org/10.1016/j.gsf.2021.101174>.
- Miller, D.M., & Lush, A.P. (1994). *Geologic map of the pilot peak quadrangle, box Elder County, Utah, and Elko County, Nevada. The Survey.*
- Miller, E.L., Gans, P.B., 1989. Cretaceous crustal structure and metamorphism in the hinterland of the Sevier thrust belt, western US Cordillera. *Geology*. 17 (1), 59–62. [https://doi.org/10.1130/0091-7613\(1989\)017.<0059:CCSAM>2.3.CO;2](https://doi.org/10.1130/0091-7613(1989)017.<0059:CCSAM>2.3.CO;2).
- Miller, E.L., Dumitru, T.A., Brown, R.W., Gans, P.B., 1999. Rapid Miocene slip on the Snake Range–Deep Creek range fault system, east-central Nevada. *Geol. Soc. Am. Bull.* 111 (6), 886–905.
- Misch, P., Hazzard, J.C., 1962. Stratigraphy and metamorphism of late Precambrian rocks in central northeastern Nevada and adjacent Utah. *Am. Assoc. Pet. Geol. Bull.* 46 (3), 289–343. <https://doi.org/10.1306/BC743823-16BE-11D7-8645000102C1865D>.
- Monroe, E.B., 2023. Doctoral dissertation. *University of California, Santa Barbara*.
- Nelson, L.L., Smith, E.F., Hodgin, E.B., Crowley, J.L., Schmitz, M.D., Macdonald, F.A., 2020. Geochronological constraints on Neoproterozoic rifting and onset of the Marinoan glaciation from the Kingston Peak Formation in Death Valley, California (USA). *Geology*. 48 (11), 1083–1087. <https://doi.org/10.1130/G47668.1>.
- Nelson, L.L., Ahm, A.S.C., Macdonald, F.A., Higgins, J.A., Smith, E.F., 2021. Fingerprinting local controls on the Neoproterozoic carbon cycle with the isotopic record of Cryogenian carbonates in the Panamint Range, California. *Earth Planet. Sci. Lett.* 566, 116956 <https://doi.org/10.1016/j.epsl.2021.116956>.
- Partin, C.A., Sadler, P.M., 2016. Slow net sediment accumulation sets snowball Earth apart from all younger glacial episodes. *Geology*. 44 (12), 1019–1022. <https://doi.org/10.1130/G38350.1>.
- Peak, B.A., Flowers, R.M., Macdonald, F.A., 2023. Ediacaran–Ordovician tectonic and geodynamic drivers of Great Unconformity exhumation on the southern Canadian Shield. *Earth Planet. Sci. Lett.* 619, 118334 <https://doi.org/10.1016/j.epsl.2023.118334>.
- Peters, S.E., Gaines, R.R., 2012. Formation of the ‘Great Unconformity’ as a trigger for the Cambrian explosion. *Nature* 484 (7394), 363–366. <https://doi.org/10.1038/nature10969>.
- Petterson, R., Prave, A.R., Wernicke, B.P., Fallick, A.E., 2011. The neoproterozoic noonday formation, Death Valley region, California. *Bulletin* 123 (7–8), 1317–1336. <https://doi.org/10.1130/B30281.1>.
- Porebski, S.J., Steel, R.J., 2003. Shelf-margin deltas: their stratigraphic significance and relation to deepwater sands. *Earth. Sci. Rev.* 62 (3–4), 283–326. [https://doi.org/10.1016/S0012-8252\(02\)00161-7](https://doi.org/10.1016/S0012-8252(02)00161-7).
- Provow, A.W., Newell, D.L., Dehler, C.M., Ault, A.K., Yonkee, W.A., Thomson, S.N., Billi, A., 2021. Revised maximum depositional age for the Ediacaran Browns Hole Formation: implications for western Laurentia Neoproterozoic stratigraphy. *Lithosphere* 2021 (1). <https://doi.org/10.2113/2021/1757114>.
- Rivers, T., 2015. Tectonic setting and evolution of the Grenville Orogen: an assessment of progress over the last 40 years. *Geosci. Canada* 42 (1), 77–124.
- Roberts, A.M., Kusznir, N.J., Corfield, R.I., Thompson, M., Woodfine, R., 2013. Integrated tectonic basin modelling as an aid to understanding deep-water rifted continental margin structure and location. *Petroleum Geosci.* 19 (1), 65–88. <https://doi.org/10.1144/petgeo2011-046>.
- Rodgers, D.W., 1984. Stratigraphy, correlation, and depositional environments of Upper Proterozoic and Lower Cambrian rocks of the southern Deep Creek Range, Utah. *Utah Geol. Assoc. Publ.* 13, 79–91.
- Rooney, A.D., Strauss, J.V., Brandon, A.D., Macdonald, F.A., 2015. A Cryogenian chronology: two long-lasting synchronous Neoproterozoic glaciations. *Geology*. 43 (5), 459–462. <https://doi.org/10.1130/G36511.1>.
- Rooney, A.D., Cantine, M.D., Bergmann, K.D., Gómez-Pérez, I., Al Baloushi, B., Boag, T. H., Strauss, J.V., 2020. Calibrating the coevolution of Ediacaran life and environment. *Proc. Natl. Acad. Sci.* 117 (29), 16824–16830. <https://doi.org/10.1073/pnas.2002918117>.
- Schneck, W.M., 1986. Doctoral dissertation. *Eastern Washington University*.
- Sloss, L.L., 1988. Tectonic evolution of the craton in Phanerozoic time. *Geol. North America* 2, 25–51.
- Smith, E.F., MacDonald, F.A., Crowley, J.L., Hodgin, E.B., Schrag, D.P., 2016. Tectonostratigraphic evolution of the c. 780–730 Ma Beck Spring Dolomite: basin Formation in the core of Rodinia. *Geol. Soc. Lond. Special Publ.* 424 (1), 213–239. <https://doi.org/10.1144/SP424.6>.
- Southwick, D.L., Morey, G.B., Mossler, J.H., 1986. Fluvial origin of the lower Proterozoic Sioux Quartzite, southwestern Minnesota. *Geol. Soc. Am. Bull.* 97 (12), 1432–1441. [https://doi.org/10.1130/0016-7606\(1986\)97.<1432:FOOTLP>2.0.CO;2](https://doi.org/10.1130/0016-7606(1986)97.<1432:FOOTLP>2.0.CO;2).
- Spencer, C.J., Hoiland, C.W., Harris, R.A., Link, P.K., Balgord, E.A., 2012. Constraining the timing and provenance of the Neoproterozoic Little Willow and Big Cottonwood Formations, Utah: expanding the sedimentary record for early rifting of Rodinia. *Precambrian Res.* 204, 57–65. <https://doi.org/10.1016/j.precamres.2012.02.009>.
- Stewart, J.H., 1974. Correlation of uppermost Precambrian and Lower Cambrian strata from southern to east-central Nevada. *US Geol. Surv. J. Res.* 2 (5), 609–618.
- Sturrock, C.P., Flowers, R.M., Macdonald, F.A., 2021. The late great unconformity of the Central Canadian Shield. *Geochem. Geophys. Geosyst.* 22 (6), e2020GC009567 <https://doi.org/10.1029/2020GC009567>.
- Talling, P.J., Masson, D.G., Sumner, E.J., Malgesini, G., 2012. Subaqueous sediment density flows: depositional processes and deposit types. *Sedimentology* 59 (7), 1937–2003. <https://doi.org/10.1111/j.1365-3091.2012.01353.x>.
- Tasistro-Hart, A.R., Macdonald, F.A., 2023. Phanerozoic flooding of North America and the great unconformity. *Proc. Natl. Acad. Sci.* 120 (37), e2309084120 <https://doi.org/10.1073/pnas.2309084120>.
- Terlaky, V., Rocheleau, J., Arnott, R.W.C., 2016. Stratal composition and stratigraphic organization of stratral elements in an ancient deep-marine basin-floor succession, Neoproterozoic Windermere Supergroup, British Columbia, Canada. *Sedimentology* 63 (1), 136–175. <https://doi.org/10.1111/sed.12222>.
- Vandyk, T.M., Kettler, C., Davies, B.J., Shields, G.A., Candy, I., Le Heron, D.P., 2021. Reassessing classic evidence for warm-based Cryogenian ice on the western Laurentian margin: the “striated pavement” of the Mineral Fork Formation, USA. *Precambrian Res.* 363, 106345 <https://doi.org/10.1016/j.precamres.2021.106345>.
- Witkosky, R., Wernicke, B.P., 2018. Subidence history of the Ediacaran Johnnie Formation and related strata of southwest Laurentia: implications for the age and duration of the Shuram isotopic excursion and animal evolution. *Geosphere* 14 (5), 2245–2276. <https://doi.org/10.1130/GES01678.1>.
- Woodward, L.A., 1963. Late Precambrian metasedimentary rocks of Egan range, Nevada. *Am. Assoc. Pet. Geol. Bull.* 47 (5), 814–822.
- Wrobel, A.J., Gans, P.B., Womer, J.B., 2021. Late Cretaceous Crustal Shortening in the Northern Snake Range Metamorphic Core Complex: constraints on the structural geometry and magnitude of pre-extensional footwall burial. *Tectonics* 40 (8), e2020TC006460. <https://doi.org/10.1029/2020TC006460>.
- Yonkee, W.A., Dehler, C.D., Link, P.K., Balgord, E.A., Keeley, J.A., Hayes, D.S., Johnston, S.M., 2014. Tectono-stratigraphic framework of Neoproterozoic to Cambrian strata, west-central US: protracted rifting, glaciation, and evolution of the North American Cordilleran margin. *Earth. Sci. Rev.* 136, 59–95. <https://doi.org/10.1016/j.earscirev.2014.05.004>.
- Zhang, T., Keller, C.B., Hoggard, M.J., Rooney, A.D., Halverson, G.P., Bergmann, K.D., Strauss, J.V., 2023. A Bayesian framework for subsidence modeling in sedimentary basins: a case study of the Tonian Akademikerbreen Group of Svalbard, Norway. *Earth Planet. Sci. Lett.* 620, 118317 <https://doi.org/10.1016/j.epsl.2023.118317>.